DOI: 10.1016/S1872-5805(22)60628-0

Recent advances in carbon materials for flexible zinc ion batteries

WU Li-sha, ZHANG Ming-hui, XU Wen, DONG Yan-feng*

(*Department of Chemistry*, *College of Sciences*, *Northeastern University*, *Shenyang* 110819, *China*)

Abstract: The ever-growing demands for wearable devices has stimulated the development of advanced flexible energy storage devices. Aqueous rechargeable zinc ion batteries (ZIBs) have gained much attention due to their low cost and intrinsic safety. Carbon materials with excellent conductivity, high mechanical strength, and light weight, can be used to construct flexible ZIBs (FZIBs). Here, we summarize the recent advances in carbon materials (e.g., carbon nanotubes, carbon fibers, graphene) for high-performance FZIBs with one-dimensional cable-shaped, two-dimensional planar, and three-dimensional sandwich configurations. Ways for constructing different types of FZIBs for better electrochemical performance are emphasized. The vital roles of carbons as the conductive materials and current collectors of cathodes, the current collectors and host materials of anodes, and modifiers of functional separators are discussed. The challenges and prospects of advanced carbon materials for next-generation FZIBs are also briefly discussed.

Key words: Carbon materials; Flexible zinc ion batteries; Cathodes; Anodes; Separators

1 Introduction

The increasing demands for flexible and wearable electronics have triggered research enthusiasm for advanced energy storage devices. Zinc metal possesses high theoretical capacity (820 mAh g^{-1} and 5 855 mAh cm^{-3}), excellent chemical stability, and low cost, enabling aqueous zinc ion batteries (ZIBs) to hold great promise in portable and bendable device applications[1, 2]. Moreover, aqueous electrolytes display high ionic conductivity (e.g., 13.31 mS cm^{-1} for 2 mol L^{-1} $ZnSO_4$[3, 4]) and environmental friendliness, and avoid the safety concerns of commercial lithium ion batteries[5]. However, amphoteric oxide cathodes of ZIBs suffer from low conductivity and poor structural stability, and the random growth of zinc dendrites may pierce through separators and lead to short-circuits, jointly causing limited energy/power density and undesirable durability[6–10]. Furthermore, flexibility is a vital indicator to define a flexible battery to bear deformations[11, 12]. In general, traditional ZIBs are constructed by metal Zn foils and cathodes consisting of active materials, conductive additives, and polymer binders on metal current collectors, and the assembled ZIBs with inferior interface interaction cannot withstand repeated mechanical deformations, such as bending, twisting, folding, and stretching. Therefore, it is highly needed to reasonably select functional materials to construct intimate interfaces to ensure rapid electron transfer and mechanical flexibility.

The pursuit for high-performance and mechanically flexible ZIBs (FZIBs) calls for the exploration of both flexible battery components (e.g., cathodes, anodes, and separators) and advanced battery configurations. Carbon materials possess high conductivity, excellent mechanical property, suitable porous structure, and light weight[13–19], which could be hybridized with active materials to achieve synergistic effects for high-performance FZIBs. Significantly, carbon materials have the ability to construct highly flexible electrodes[20, 21], and the absence of polymer binders and additional conductive additives can not only simplify the fabrication procedures but also remarkably enhance the energy density of corresponding FZIBs. Notably, carbon materials are highly desired for the development of various flexible battery configurations, involving 1D cable-shaped[22, 23], 2D planar[24, 25], and 3D sandwiched batteries[26, 27], in which both active materials/current collectors and electrodes/electrolytes interfaces are stable and robust enough to with-

Received date: 2022-06-06; **Revised date:** 2022-07-12

Corresponding author: DONG Yan-feng, Associate Professor. E-mail: dongyanfeng@mail.neu.edu.cn

Author introduction: WU Li-sha, Master Student. E-mail: 1970065@stu.neu.edu.cn

stand repeated deformations, thus ensuring the integrity of FZIBs to work normally. In this regard, carbon materials play great roles in constructing high-performance FZIBs. However, there is still a lack of a timely and latest review to keep pace with the surging development of FZIBs.

Herein, we summarize the recent progress of carbon materials (e.g., graphene, carbon nanotubes (CNTs), and carbon fibers) for FZIBs with different battery configurations, such as the 1D cable-shaped, 2D planar, and 3D sandwiched FZIBs, and the vital roles of carbon materials have been elaborated as conductive materials and current collectors for cathodes, current collectors and host materials for Zn anodes, and modifiers for functional separators (Fig. 1). Especially, the construction strategies of carbon-based FZIBs and the enhanced flexibility and electrochemical performance are emphasized. Finally, prospects on carbon materials for advanced FZIBs are also briefly discussed.

2 Configurations of FZIBs

Before we introduce the progress of various carbon materials for FZIBs, 1D cable-shaped FZIBs, 2D planar FZIBs, and 3D sandwiched FZIBs are firstly clarified based on the configurations of FZIBs. Obviously, different strategies should be applied to construct specific configuration of FZIBs. Therefore, it is necessary to briefly introduce the unique features and differences of the three configurations.

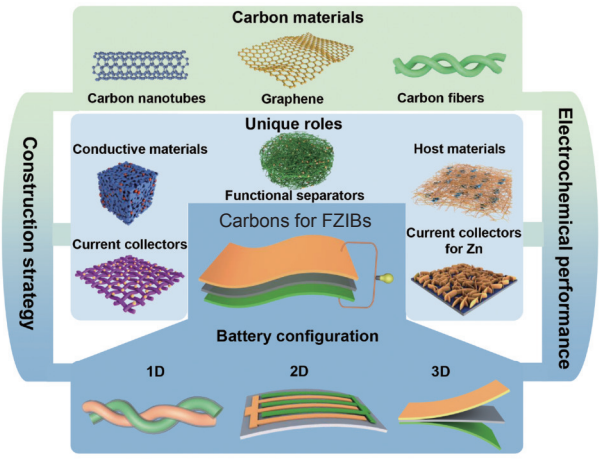

Fig. 1 Schematic illustration of various carbon materials for FZIBs.

2.1 1D cable-shaped FZIBs

Generally, 1D cable-shaped FZIBs can be categorized into the coaxial type and twisted structure according to the connection pattern of cathodes and anodes[22]. In coaxial FZIBs (Fig. 2a), the core electrode is usually wrapped by a separator, which is further as a substrate for the synthesis of outer electrode, resulting in a core-shell structure. As for the twisted structure (Fig. 2b), a cathode fiber and an anode fiber are intertwined together into a double-helix structure[28]. Notably, the key to construct such 1D cable-shaped FZIBs is to prepare 1D Zn anodes. Obviously, commercial Zn fibers can be directly employed as core anodes, however, metal Zn fibers may suffer from metal fatigue after repeated bending cycles. Alternatively, Zn on conductive fiber-shaped substrates can be fabricated via electrochemical deposition route, and in this regard, conductive carbon nanomaterials undoubtedly play great roles to construct 1D cable-shaped FZIBs. Importantly, the cable-shaped FZIBs could be integrated with elastic substrates to achieve excellent stretchability (Fig. 2c). Meanwhile, 1D cable-shaped FZIBs usually display miniaturization, light weight, and exceptional flexibility, and they can be deformed into any states and even woven into fabrics, making them suitable to construct wearable and flexible electronics (Fig. 2d). Such configuration of FZIBs can be further integrated with industrial textile technologies, showing promising application in future wearable devices[29–32].

2.2 2D planar FZIBs

The 2D planar FZIBs can be fabricated on a variety of flexible substrates (e.g., cloth, polyethylene terephthalate (PET), and paper) for the construction of highly flexible structures. For a 2D planar battery, the cathode and anode are positioned side by side with insulated gaps lying between adjacent finger microelectrodes, avoiding the usage of additional separators (Fig. 2e)[33]. Furthermore, electrolytes are placed on the top of or embedded in microelectrodes, which significantly provides large active area and reduces ion transfer resistance[34]. Moreover, electrolyte ions transfer in a transverse direction, enabling efficient ion diffusion even with the increase of the battery thickness. Meanwhile, several 2D planar batteries can be easily

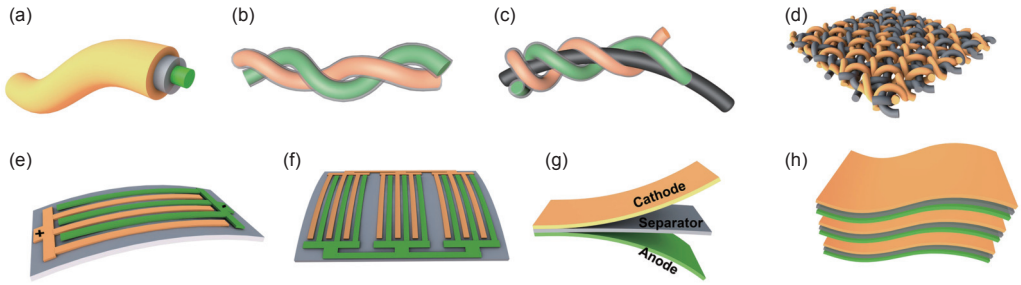

Fig. 2　Configurations and integration of FZIBs. (a) 1D coaxial battery. (b) 1D twisted battery. (c) 1D stretchable battery. (d) 1D cable-shaped batteries could be woven into fabrics. (e) 2D planar battery. (f) Three planar batteries could be connected in parallel for practical applications. (g) 3D sandwiched battery. (h) Three sandwiched batteries could be connected in series for practical applications.

connected in serial or in parallel on planar substrates, favoring the achievement of high energy and power density for powering ultrathin energy-consuming devices (e.g., electrical display screen) (Fig. 2f)[35]. In addition, the 2D planar battery could be integrated with microelectronics[36] (e.g., solar cells[37], sensors[38]) to achieve the generation and use of power without delay for extended promising applications[39]. By virtue of the unique interdigital structure and flexible substrates, the 2D planar FZIBs possess great mechanical robustness and simultaneously avoid the short-circuit issues under deformation conditions.

2.3　3D sandwiched FZIBs

3D sandwiched FZIB is one of the most widely applied configurations. In this structure, liquid electrolytes in separators or solid electrolytes are sandwiched between cathode and anode (Fig. 2g), and the face-to-face contact mode between electrodes and electrolyte realizes efficient ion diffusion and endows stable interfaces[33]. Moreover, sandwiched FZIBs could be easily stacked face to face to power various electronics (Fig. 2h). Theoretically, the 3D sandwiched FZIBs require the introduction of flexible electrodes or electrolytes. Flexible and lightweight carbon substrates are generally employed for the direct growth of active materials to construct flexible electrodes, while in traditional ZIBs, heavy and smooth metal current collectors (e.g., stainless steel foil, Ti foils) are usually used, in which active materials tend to fall off metal substrates under deformations due to poor interface interaction. Moreover, to ensure the stable connection between active materials and current collectors, free-standing and flexible carbon based films are frequently employed for FZIBs without the employment of polymer binders or conductive additives.

The 1D cable-shaped, 2D planar, and 3D sandwiched FZIBs show glimpses of a future where wearable and portable electronics powered by FZIBs could fulfill the practical and customized requirements in our daily life.

3　Carbons in cathodes

Various conductive carbon materials can be paired with cathode active materials (e.g., MnO_2, V_2O_5) for the construction of FZIBs, in which synergistic effects of both components can be expected to enhance electrochemical performance and exceptional flexibility. To be specific, the vital roles of carbon materials in cathodes lie in the following two aspects:

(1) Conductive materials. The intimate connection between carbons and active materials endows the composite cathodes with rapid electron transfer pathways and robust structure to accommodate volume variation during Zn^{2+} insertion/extraction processes. Moreover, carbon materials could be assembled with active materials to obtain free-standing binder-free films for highly flexible cathodes and FZIBs.

(2) Current collectors. They could not only accelerate electron transfer but also ensure high mechanical flexibility due to the presence of flexible and conductive substrates. Notably, lightweight carbon-based current collectors have the ability to accommodate high-mass-loading active materials (e.g., 15 mg cm^{-2}), which helps to achieve high-energy-density cathodes for FZIBs.

To fully understand the roles of carbons in different battery configurations, various cathodes in FZIBs are summarized in Table 1.

Table 1 A summary of carbon based cathodes for FZIBs.

Role of carbons	Battery configu rationsns	Cathode	Anode	Electrolyte	Voltage window	Capacity	Capacity retention	Energy/ power density	Flexibility	Ref.
Conductive materials	1D cable-shaped	MnO_2/CNFs-CNTs	Zn/CNFs-CNTs	2 M $ZnSO_4$ + 0.1 M $MnSO_4$	0.8–1.9 V	281.5 mAh g^{-1} 0.25 A g^{-1}	65.7% (400 cycles)	47.3 Wh kg^{-1} 42.2 W kg^{-1} ($E_{electrode}$)	Bent, looped, twisted, typed	[40]
	2D planar	CNT@MnO_2	Zinc powder	1 M $ZnSO_4$ + 0.1 M $MnSO_4$	0.8–1.8 V	63 μAh cm^{-2} 0.4 mA cm^{-2}	94.6% (87 cycles)	404.3 Wh kg^{-1} 135.2 W kg^{-1}	Bent	[41]
	2D planar	A-V_2O_5/G	Zn powder	3 M $ZnSO_4$	0.2–1.8 V	20 mAh cm^{-3} 1 mA cm^{-2}	80% (3500 cycles)	21 mWh cm^{-3} 526 mW cm^{-3}	Bent, twisted	[42]
	2D planar	VO_2 (B)-MWCNTs	Zinc nanoflakes	2 M $Zn(CF_3SO_3)_2$	0–2 V	314.7 μAh cm^{-2} 0.14 mA cm^{-2}	71.8% (200 cycles)	188.8 μWh cm^{-2} 0.09 mW cm^{-2}	Bent	[25]
	3D sandwiched	CuV_2O_6/RCNTs	Zn foil	2/3 M $Zn(CF_3SO_3)_2$	0.3–1.5 V	353 mAh g^{-1} 0.1 A g^{-1}	61.5% (1400 cycles)	353 Wh kg^{-1} 90 W kg^{-1}	Bent	[43]
	3D sandwiched	$H_{0.08}MnO_2 \cdot 0.7H_2O$/ MWCNT membrane	Zn foil	2 M $ZnSO_4$ + 0.2 M $MnSO_4$	1.0–1.9 V	276.3 mAh g^{-1} 0.2 A g^{-1}	80.8% (1000 cycles)	368.3 Wh kg^{-1} 300 W kg^{-1} ($E_{material}$)	Bent	[44]
	3D sandwiched	KVO/SWCNT	Zn foils	4 M $Zn(CF_3SO_3)_2$	0.3–1.3 V	379 mAh g^{-1} 0.1 A g^{-1}	91% (10000 cycles)	–	Bent	[45]
	3D sandwiched	PANI/SWCNTs	Zn/SWCNTs-rGO	PVA-$Zn(CF_3SO_3)_2$	0.5–1.5 V	167.6 mAh g^{-1} 0.1 A g^{-1}	97.3% (1000 cycles)	–	Bent, stretchable	[46]
	3D sandwiched	a-MnO_2@CNT foams	Zn@CNT	2 M $ZnSO_4$/ 0.2 M $MnSO_4$	1.0–1.8 V	308.5 mAh g^{-1} 0.97 C	100% (1000 cycles)	–	Bent	[47]
	3D sandwiched	h-CNT/PANI	Zn foil	2 M $ZnSO_4$	0.5–1.5 V	97 mAh g^{-1} 0.1 A g^{-1}	105.8% (1000 cycles)	104 Wh kg^{-1}/ 8.3 kW kg^{-1}	Bent	[48]
	3D sandwiched	MnO_2/rGO	Zn foil	2.0 M $ZnSO_4$ + 0.1 M $MnSO_4$	1.0–1.9 V	317 mAh g^{-1} 0.1 A g^{-1}	78% (2000 cycles)	436 Wh kg^{-1} ($E_{cathode}$)	Bent, folded	[49]
	3D sandwiched	VO_2/rGO	Zn foil	3M $Zn(CF_3SO_3)_2$	0.3–1.3 V	276 mAh g^{-1} 0.1 A g^{-1}	99% (1000 cycles)	65 Wh kg^{-1} 7.8 kW kg^{-1}	Bent	[50]
	3D sandwiched	MnO/G	Zn foil	2 M $ZnSO_4$ + 0.1 M $MnSO_4$	1–1.85 V	398.5 mAh g^{-1} 0.1 A g^{-1}	70% (2000 cycles)	–	Bent	[51]
Current collectors	1D cable-shaped	MnO_2@CNT	Zn wire	1.5 M LiCl-2M $ZnCl_2$-PVA	1.0–1.8 V	290 mAh g^{-1} 0.1 A g^{-1}	75% (300 cycles)	360 Wh Kg^{-1} 100 W Kg^{-1} ($E_{material}$)	Folded	[52]
	1D cable-shaped	CNT-stitched ZVO NSs@OCNT	Zn NSs@CNTs fiber	CMC/$ZnSO_4$ polymer gel electrolyte	0.2–1.8 V	114 mAh cm^{-3} 0.1 A cm^{-3}	88.6% (2000 cycles)	71.6 mWh cm^{-3} 0.071 W cm^{-3} (E_{device})	Bent	[53]
	1D cable-shaped	Co_3O_4 NSs@CNTF	Zn NSs@CNTF	2 M $ZnSO_4$ + 0.0005 M $CoSO_4$	0.8–2.1 V	158.70 mAh g^{-1} 1 A g^{-1}	97.27% (10000 cycles)	–	Bent	[54]
	1D cable-shaped	ZnHCF@CNTs	Zn nanosheet arrays on CNTFs	$ZnSO_4$-CMC gel	1.0–2.1 V	100.2 mAh cm^{-3} 0.1 A cm^{-3}	91.8% (200 cycles)	195.4 mWh cm^{-3} 0.2 W cm^{-3}	Bent	[55]
	3D sandwiched	CNT@MnO_2	Zn foil	2 M $ZnSO_4$ + 0.2 M $MnSO_4$	1–1.85 V	292.7 mAh g^{-1} 0.2 mA cm^{-2}	100% (1000 cycles)	16.5 mWh cm^{-3} 10.3 mW cm^{-3}	Bent	[56]
	3D sandwiched	MnO_2/CNT	zinc nanosheet based textile	$ZnSO_4$+$MnSO_4$	1.0–1.8 V	138.8 mAh g^{-1} 1 C	91% (1000 cycles)	12 mWh cm^{-3} 13 mW cm^{-3} (E_{device})	Bent	[57]
	3D sandwiched	MnO_2/CNT foam	Zn foil	2 M $ZnSO_4$ + 0.005 M $MnSO_4$	1.0–2.4 V	0.332 mAh cm^{-2} 2 mA cm^{-2}	100% (16000 cycles)	602 Wh kg^{-1} ($E_{material}$)	–	[58]
	3D sandwiched	Al_2O_3@VSe_2 NSs@N-CNFs	Zn NSs@CNT	$ZnSO_4$	0.3–1.5 V	495.4 mAh g^{-1} 0.05 A g^{-1}	86.2% (2500 cycles)	362.5 Wh kg^{-1} 44 W kg^{-1}	Bent	[59]
	3D sandwiched	VO_2 (B)@CFS	Zn foil	1 M $ZnSO_4$	0.2–1.2 V	386.2 mAh g^{-1} 0.2 A g^{-1}	65.5% (1000 cycles)	–	Bent	[60]
	3D sandwiched	VS_2/CC	Zn/CC	PVA-Zn/Mn hydrogel	0.4–1.0 V	175 mAh g^{-1} 0.2 A g^{-1}	70.3% (40 cycles)	–	Bent	[61]
	3D sandwiched	ZnVOH/CC	Zn/CC	3 M $Zn(CF_3SO_3)_2$	0.2–1.4 V	337 mAh g^{-1} 1.0 A g^{-1}	94.6% (5000 cycles)	–	Rolled, folded, punched	[62]
	3D sandwiched	O_d-Mn_3O_4@C NA/CC	Zn foil	2 M $ZnSO_4$ + 0.2 M $MnSO_4$	0.2–1.8 V	396.2 mAh g^{-1} 0.2 A g^{-1}	95.7% (12000 cycles)	537.5 Wh kg^{-1} 268.75 W kg^{-1}	–	[63]
	3D sandwiched	N-CNSs@MnO_2	N-CNSs@Zn	2 M $ZnSO_4$ + 0.2 M $MnSO_4$	1.0–1.8 V	271.2 mAh g^{-1} 0.5 A g^{-1}	76.5% (500 cycles)	352.5 Wh kg^{-1} 542.4 W kg^{-1}	Bent, twisted	[64]
	3D sandwiched	MnO_2/CC	Zn foil	2 M $ZnSO_4$ + 0.1 M $MnSO_4$	0.8–1.8 V	212.8 mAh g^{-1} 1 A g^{-1}	124% (300 cycles)	–	Bent	[65]
	3D sandwiched	C-MnO_2@CC	Zn/CC	2 M $ZnSO_4$ + 0.2 M $MnSO_4$	0.8–1.9 V	1.3 mAh cm^{-2} 1.0 A cm^{-2}	86.5% (10000 cycles)	1.34 mWh cm^{-2} 2.95 mW cm^{-2}	Bent, twisted	[66]
	3D sandwiched	MnO_2/CF	Zn/CF	PVA/$ZnCl_2$-$MnSO_4$	0.8–2.0 V	145.9 mAh g^{-1} 0.1 A g^{-1}	88.3% (100 cycles)	181.5 Wh kg^{-1} 0.31 kW kg^{-1} ($E_{material}$)	Tensile, bent, compressed	[67]
	3D sandwiched	CuMO	Zn foil	2 M $ZnSO_4$ + 0.2 M $MnSO_4$	0.8–1.9 V	398.2 mAh g^{-1} 0.1 A g^{-1}	90.1% (700 cycles)	156 Wh kg^{-1} 6250 W kg^{-1}	Bent	[27]
	3D sandwiched	FSM@FGF	Zn metal	1/2 M $ZnSO_4$	1.0–1.9 V	440.1 mAh g^{-1} 0.1 A g^{-1}	82.7% (300 cycles)	396 Wh kg^{-1} 90 W kg^{-1}	Folded in water	[68]

Note: M: mol L^{-1}

3.1 Conductive materials

3.1.1 Carbon nanotubes

1D carbon nanotubes with high conductivity (~ 5×10^5 S m^{-1}) are widely applied to integrate with active materials[69, 70]. Notably, CNTs can be intertwined into interconnected conductive networks, forming free-standing and flexible films without the need of extra conductive additives and polymer binders, and thus the uniform dispersion and the utilization of active materials are greatly improved.

Generally, CNTs could be directly vacuum filtrated with active materials to obtain free-standing and binder-free composite cathodes. Typically, VO_2 (B) nanofibers with a length of a few microns were reported to be vacuum filtrated with multiwalled CNTs (MWCNTs) for free-standing VO_2 (B)-MWCNT films (Fig. 3a), which were further treated with laser engraving process for finger electrodes. The constructed 2D planar FZIBs delivered a favorable energy density of 188.8 μWh cm^{-2} at a power density of 0.09 mW cm^{-2} and realized high mechanical and heat stability under bending states (0°-150°) (Fig. 3b) and a temperature range of 25-100 °C (Fig. 3c)[25]. V_2O_5/CNT porous composite films were fabricated as flexible cathodes through vacuum filtration, in which V_2O_5 nanofibers were interpenetrated in the CNT network for enhanced electron/ion transfer. As expected, a high diffusion coefficient of Zn^{2+} (~ 10^{-8} cm^2 s^{-1}) was achieved and a reversible capacity of 390 mAh g^{-1} was delivered at 1 A g^{-1}, much higher than pure V_2O_5 (263 mAh g^{-1})[71]. Moreover, metal ions or water molecules pre-insertion is considered as an ef-

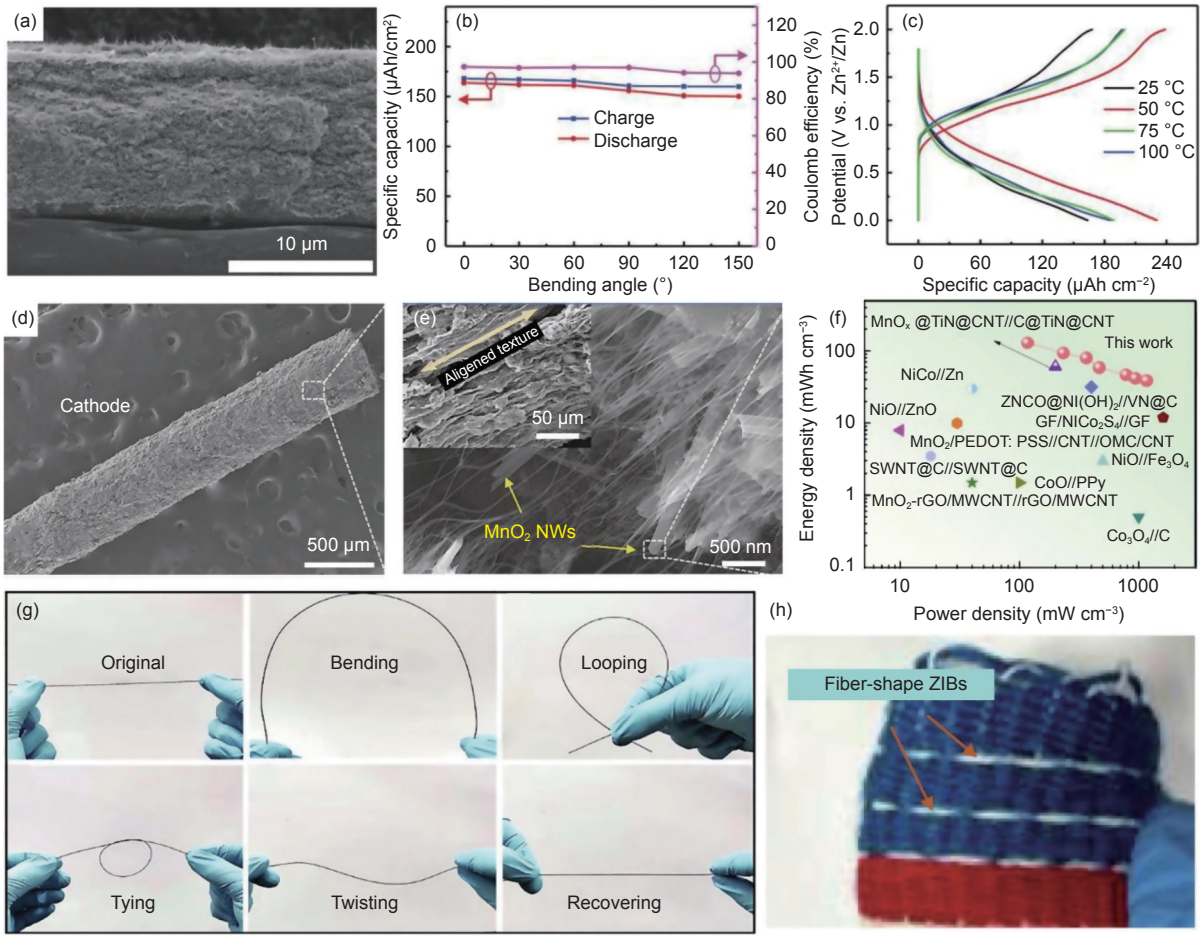

Fig. 3　(a) Cross-sectional scanning electron microscope (SEM) image of VO_2 (B)-MWCNT cathode. (b) Specific capacity and Coulombic efficiency of FZIBs under various bending angles. (c) Galvanostatic charge/discharge (GCD) curves of FZIBs at different temperatures[25]. Reprinted with permission by copyright 2019, Wiley. (d, e) SEM images of the MnO_2/CNF-CNT fiber cathode. (f) Ragone plot of the 1D FZIBs based on the MnO_2/CNF-CNT cathode in comparison with previously reported fiber-shaped energy storage devices. (g) Flexible fiber electrodes under various deformations. (h) Digital photograph showing that FZIBs could be woven into textile for potential practical applications[40]. Reprinted with permission by copyright 2022, Elsevier.

fective method to enlarge interlayer spacing for enhancing structural integrity[10]. For example, CuV_2O_6 nanobelts were hydrothermally synthesized and subsequently vacuum filtrated with reductive acidified CNTs (RCNTs) featuring enhanced conductivity and hydrophilicity, achieving a free-standing and binder-free composite membrane. High-aspect-ratio CuV_2O_6 and robust RCNT network can be homogeneously and tightly interconnected, resulting in highly flexible films that can be bent without any obvious cracks[43]. Moreover, rGO/$Na_xV_2O_5{\cdot}nH_2O$ (rGO/NVO), CNTs, and cellulose fibers were assembled into a free-standing nanocomposite paper with a thickness of ~ 100 μm. Specially, the rGO/NVO possessed a large interlayer spacing of 1.06 nm due to the presence of Na^+ and water molecules, which could stabilize the V_2O_5 crystal structure and ensure rapid Zn^{2+} diffusion. Meanwhile, the continuous CNT framework enabled a high conductivity of 784 S m^{-1} for the nanocomposite, and the cellulose fibers functioned both as a building block to realize flexible thick film electrodes and electrolyte reservoir for rapid ion transfer. Consequently, the paper cathode exhibited a high tensile strength of 8.51 MPa, and the assembled rGO/NVO based ZIB delivered a high areal capacity of 1.87 mAh cm^{-2} even at a high mass loading of 5 mg cm^{-2}[72]. Similarly, single-walled CNTs (SWCNTs) and hydrophilic cellulose nanofibers could be assembled into a 3D bicontinuous heterofibrous network scaffold (HNS), which enabled the uniform distribution of active α-MnO_2 rods in the HNS and the construction of free-standing MnO_2/HNS cathodes through vacuum filtration and freeze-drying process. Significantly, the porous and conductive HNS network provided continuous electron/ion transfer pathways to achieve excellent mechanical flexibility and simultaneously accelerated redox kinetics, thus endowing the corresponding ZIBs with an unchanged electronic resistance after 5 000 bending cycles, an excellent rate capability of 129 mAh g^{-1} at 20 C, and a high energy ($E_{electrode}$)/power density ($P_{electrode}$) of 91 Wh kg^{-1}/1 848 W kg^{-1}[73]. Besides, proton-type birnessite $H_{0.08}MnO_2{\cdot}0.7H_2O$ nanobelts possessing a high aspect ratio of ~ 30 were reported to integrate with MWCNTs by vacuum filtration, and the as-fabricated binder-free $H_{0.08}MnO_2{\cdot}0.7H_2O$/MWCNT film possessed robust structure and abundant macropores (0.5-5.0 μm) to avoid the self-stacking of active materials, alleviate volume variations, and facilitate the infiltration of electrolyte ions into electrodes, and thus enabled a high Zn^{2+} diffusion coefficient of ~ 8.18×10^{-14} cm^2 s^{-1} and a long-term life up to 1 000 cycles at 3 A g^{-1}[44].

Moreover, other physical assembly strategies (e.g., spray printing, wet spinning, blade coating and rolling assembly) are also developed to enable the successful construction of FZIBs. Typically, $KV_3O_8{\cdot}0.75H_2O$ (KVO) nanobelts with the V^{3+}/V^{5+} redox reaction and large interlayer spacing were hydrothermally prepared, which were subsequently subjected to assembly with SWCNTs in a spray printing process to achieve free-standing KVO/SWCNT composite films featuring a thickness of 8 μm. KVO nanobelts were well distributed in the CNT network, resulting in a conductive structure and exceptional flexibility for the composite film. Notably, the film can be bent to 180° without any cracks and structural damage. Simultaneously, the 3D sandwiched FZIBs could deliver almost an unchanged discharge capacity of ~ 210 mAh g^{-1} at 1 A g^{-1} for 200 cycles under either flat or bent conditions[45]. In addition, wet spinning is a low-cost and scalable strategy to fabricate fiber-shaped electrodes. For instance, CNTs, cellulose nanofibers (CNFs), and MnO_2 nanowires could be mixed as viscous spinning inks, and after wet spinning in the ethanol coagulation bath, the composite cathode was constructed, in which CNTs and CNFs with high aspect ratio and large specific surface area (SSA) were interconnected into a binary fibrous network for the uniform interpenetration of MnO_2 nanowires (Fig. 3d, e). As demonstrated, the 1D fiber-shaped FZIB delivered high gravimetric and volumetric energy densities ($E_{electrode}$) of 47.3 Wh kg^{-1} and 131.3 mWh cm^{-3} at 42.2 W kg^{-1} at 117.3 mW cm^{-3}, respectively (Fig. 3f), and achieved excellent flexibility to maintain a high capacity retention of 92% after 4 000 bending cycles at the largest bending angle of 90°. Moreover, the flexible fiber electrodes could be bent, looped, typed, and twisted (Fig. 3g), thus endowing

the 1D FZIBs with favorable flexibility and mechanical strength to be woven into flexible textiles for practical applications (Fig. 3h)[40]. Besides, blade coating and rolling assembly hold great promise for the fabrication of all-in-one integrated ZIBs with high flexibility. Niu and co-workers[46] developed polyaniline (PANI) nanorods that could be cross-linked with SWCNTs, and the resulting composite slurry was spread over a polyimide substrate through blade coating to obtain porous PANI/SWCNT composite films with a high conductivity of 1 730 S m^{-1}. Significantly, the unique integrated structure of combining all components into one monolith reduced ion transfer distance and ensured structural compatibility and intimate interfacial connection. Correspondingly, the 3D all-in-one FZIB showed an elastic strain of ~12.9% with a Young's modulus of ~34.5 MPa, and could deliver stable capacity under various stretching conditions. Moreover, the constructed FZIBs could be tailored into various desired shapes for the exploration of stretchable, editable and shape-customized configurations.

Chemical assembly can construct a composite structure of CNTs and active materials with strong adhesion, and thus obtaining highly flexible and stable cathodes. Typically, after acid treatment, hydrophilic CNTs acted as a template to reduce $KMnO_4$ and as a conductive substrate to support the uniform dispersion of amorphous MnO_2 nanosheets. The synergy of the porous CNT network and amorphous MnO_2 with the highly disordered structure provided more active sites and accelerated ion diffusion and reaction kinetics, endowing the free-standing a-MnO_2@CNT foams with attractive rate performance, such as a reversible specific capacity of 69.5 mAh g^{-1} at 97.4 C. Significantly, the FZIB delivered a stable specific capacity of 180.7 mAh g^{-1} at 6.5 C under flat state, and maintained 179.0 mAh g^{-1} under various bent conditions, indicative of high mechanical flexibility[47]. Similarly, MnO_2 nanosheets were hydrothermally assembled on the surface of CNTs to construct a cross-linked hierarchical framework, and the resulted CNT@MnO_2 ink was 3D-printed on substrates in a precise manner for 2D planar FZIBs, which delivered a stable reversible capacity of 63 μAh cm^{-2} at 0.4 mA cm^{-2} and maintained 97.28% of initial capacity under bending states[41]. In addition, bilayered $Na_xV_2O_5{\cdot}nH_2O$ (NVO) nanobelts with Na^+ ions and water molecules as pillars embedded in V_2O_5 framework possessed a larger interlayer spacing of ~1.1 nm than pure V_2O_5 (~0.44 nm), thus accommodating more Zn^{2+} and favoring reaction kinetics. CNT networks as structure-direction agent could guide the hydrothermal growth of NVO nanobelts by providing active sites (e.g., oxygen-containing groups and defects) on the surface of CNTs. In the resulted free-standing and binder-free NVO@CNTs composite films, active NVO nanobelts and conductive CNTs were interwoven and well distributed to form a porous and conductive structure, enlarging the contact area between active materials and electrolytes, and enhancing reaction kinetics. As expected, the NVO@CNT composite delivered a high capacity of 330.5 mAh g^{-1} at 2 A g^{-1} at a high mass loading of 12 mg cm^{-2}[74].

Besides, some polymers (e.g., polydopamine, polyaniline) can be self-polymerized on the surface of CNTs with strong interaction, thus achieving stable interface between CNTs and active materials to withstand repeated charge/discharge and various deformations. For instance, polydopamine (PDA) possesses both hydrophilic nature for fast ion diffusion at electrode/electrolyte interface and low solubility in aqueous solutions to avoid the dissolution issues. To further stabilize the structure and enhance conductivity, CNTs were selected as substrates for the self-polymerization of dopamine, resulting in a robust interface with strong adhesion. After vacuum filtration, the PDA coated CNTs with a thickness of 8 nm was well-interwoven into a flexible and high-rate PDA/CNT membrane. Therefore, based on catechol/ortho-quinone redox reactions and Zn^{2+} adsorption/desorption, the PDA/CNT cathode delivered a high capacity of 126.2 mAh g^{-1} and maintained 96% of initial capacity after 500 cycles[75]. More interestingly, highly conductive CNTs with length of hundreds of nanometers can be modified with various oxygen-containing functional groups, —OH in particular, to enhance wettability and Zn^{2+} storage capability by introducing chemical adsorption into original

electric double-layer capacitance. Furthermore, PANI with active redox sites and high chemical stability was in situ polymerized on the surface of hydroxylated CNTs (h-CNT), resulting in a h-CNT/PANI composite cathode. The integration of capacitive chemical adsorption of h-CNTs with redox reactions on PANI endowed the h-CNT/PANI composite cathode with a superior capacity retention of 49% as the current density increased from 0.1 to 5 A g^{-1} to pure PANI cathode (6.2%). Moreover, the constructed FZIB delivered a capacity retention of 90% after bending for 600 cycles, which sheds light on the great flexibility benefiting from the presence of CNT network[48].

3.1.2 Graphene

Graphene nanosheets possess a unique 2D ultrathin structure and physicochemical properties, such as superior conductivity (~107 S m^{-1}), large SSA (~2 630 m^2 g^{-1}), and exceptional mechanical strength[6, 76], which are promising conductive materials for advanced FZIBs with enhanced battery performance[50, 77]. Moreover, nano graphene could assemble with active materials into conductive and flexible composite films, which avoids the self-stacking of graphene nanosheets and agglomeration of active materials[78]. Most importantly, graphene nanosheets can be easily assembled into 1D fibers, 2D films and 3D aerogels. With the rapid development of graphene industry, advanced and low-cost graphene based hybrids are expected to be massively produced for practical applications.

Vacuum filtration is also frequently employed to achieve graphene based composite cathodes with enhanced reaction kinetics and desirable flexibility. As a typical example, 1D ultralong MnO_2 nanowires with high aspect ratios of above 1 000 were reported to be assembled with rGO nanosheets without restacking to obtain a lightweight MnO_2/rGO hybrid membrane (Fig. 4a). Notably, the 1D/2D hybrid structure with a

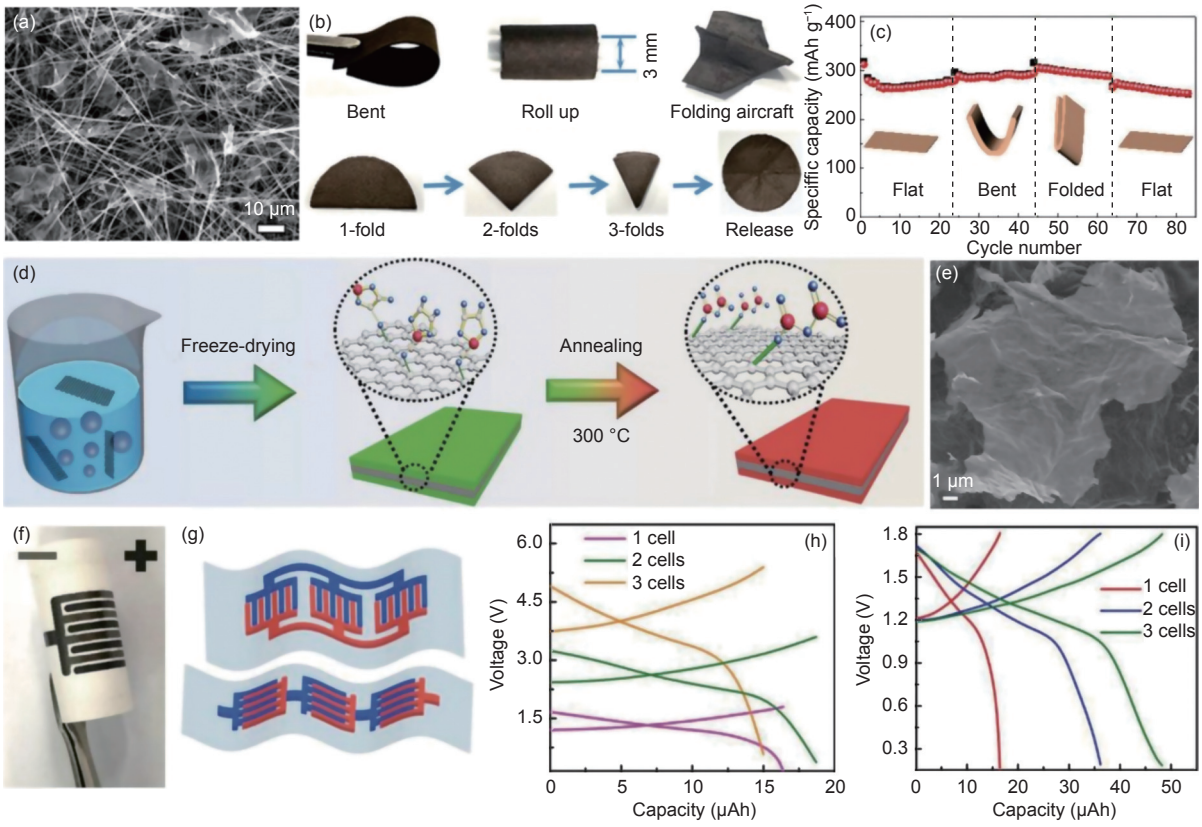

Fig. 4 (a) SEM image of MnO_2/rGO composite. (b) Digital photograph exhibiting flexible MnO_2/rGO membrane to bear various deformations such as bending, rolling, and folding. (c) Cycling performance of FZIB under different deformations[49]. Reprinted with permission by copyright 2020, Wiley. (d) A schematic of the preparation of 2D A-V_2O_5/G heterostructures. (e) SEM image of A-V_2O_5/G heterostructures. (f) Digital photograph of the 2D planar FZIB. (g) Schematic illustration of three FZIBs connected in series or parallel. (h, i) GCD curves of FZIBs connected (h) in series or (i) in parallel from 1 to 3 batteries[42]. Reprinted with permission by copyright 2020, Wiley.

high SSA of 159.9 m^2 g^{-1} not only reduced line-to-face ion pathways for fast reaction kinetics, but also enabled the films with extraordinary mechanical flexibility, such as abilities to bear bending, rolling, and multiple folding (Fig. 4b). Consequently, the constructed FZIBs could operate stably and exhibit unchanged reversible redox reactions under flat, bent or even folded conditions (Fig. 4c)[49].

The chemical assembly of rGO and vanadium or manganese based oxides can be achieved through calcination of graphene oxides (GO) and vanadium or manganese based precursors. Recently, amorphous V_2O_5 grew on both sides of graphene nanosheets through freeze-drying of VOC_2O_4 and GO and subsequent calcination (Fig. 4d), resulting in a flat and ultrathin 2D A-V_2O_5/G heterostructure (Fig. 4e), which ensured superior structural stability and offered ion diffusion tunnels for fast electron/ion transfer. Moreover, amorphous V_2O_5 with a disordered structure provided abundant active sites for H^+/Zn^{2+} insertion/extraction. Accordingly, a 2D planar FZIB was constructed by a vacuum filtration method (Fig. 4f), which delivered an excellent energy density of 21 mWh cm^{-3} at 526 mW cm^{-3}, and three FZIBs connected in series and parallel exhibited stable charge/discharge processes (Fig. 4g-i), demonstrative of great potential in miniature electronics[42]. Similarly, active VO_2 could be decorated on graphene framework through freeze-drying and subsequent calcination of a mixture of GO and NH_4VO_3, during which GO was reduced to rGO and meanwhile NH_4VO_3 was converted to VO_2 via the reaction of $NH_4VO_3 + C \rightarrow NH_3\uparrow + VO_2 + CO_2\uparrow + H_2O\uparrow$. After mechanical compression, the VO_2/rGO composite film was obtained, which possessed both a high SSA of 251 m^2 g^{-1} for the easy infiltration of electrolyte ions and a porous structure to ease volume variations caused by ion insertion/de-insertion. The robust VO_2 and conductive and porous rGO network synergistically improved the electrochemical performance of 3D sandwiched FZIBs, such as reversible capacities of 260 and 194 mAh g^{-1} at 0.2 and 8 A g^{-1}, respectively, and stable operation for 200 cycles without obvious capacity decay at varied bending radius from 4.0 cm to 1.0 cm, demonstrative of great potential in wearable electronics[50]. In addition, through calcination of a mixture of MnO_2 and GO, MnO were densely decorated between graphene layers to form accordion-like MnO/G heterostructures. The graphene-MnO interphase in MnO/G connected with covalent bonds ensured structural stability and provided rich active sites for reduced Zn^{2+} adsorption energy and favorable Zn^{2+} storage due to the formation of oxygen vacancies in disordered MnO, thus resulting in a high capacity of 398.5 mAh g^{-1} at 0.1 A g^{-1}[51]. In addition, layered MoS_2 was also reported to be integrated with graphene to construct sandwich-structured MoS_2/graphene nanosheets through electrostatic assembly and subsequent hydrothermal reduction, in which the presence of graphene effectively enlarged the interlayer of MoS_2 from 0.62 to 1.16 nm. Importantly, the synergy of graphene and MoS_2 resulted in enhanced hydrophilicity and high structural stability, and thus enabled high capacities of 285.4 and 141.6 mAh g^{-1} at 0.05 and 5 A g^{-1}, respectively, and a high capacity retention of 88.2% after 1 800 cycles[77].

3.2 Current collectors

3.2.1 Carbon nanotubes

Individual CNTs can be highly aligned into interconnected network featuring a robust structure, high conductivity, and high mechanical strength, which is desirable for current collectors in flexible cathodes. Typically, molten V_2O_5 under the heating temperature of 800 °C could intimately infiltrate the porous framework of CNT films (CNTFs), forming CNTF/V_2O_5 films with high chemical stability and compact structure. Notably, the structurally stable and flexible CNTF@V_2O_5 composite film would not re-disperse in water even under ultrasonication for 1 h and could sustain structural integrity without cracks under frequent folded or crumped states. As a result, the corresponding ZIB delivered a reversible capacity of 356.6 mAh g^{-1} at 0.4 A g^{-1} and high capacity retention of 80.1% after 500 cycles at 2.0 A g^{-1}[79]. Moreover, Xu and co-workers[56] electrodeposited MnO_2 nanoflakes on CNT films to obtain a binder-

free CNT@MnO_2 film, in which MnO_2 nanoflakes were densely and uniformly distributed on the surface of CNT threads. The synergy of conductive CNT substrate and nanostructured MnO_2 contributed to high-performance of 3D Zn//MnO_2 flexible batteries, such as a high energy density up to 16.5 mWh cm^{-3} at 0.2 mA cm^{-2} and long cycling life over 1 000 times without obvious capacity decay. Furthermore, CNT layers were reported to be coated on the surface of flexible textiles by a dipping-drying method to dramatically enhance the conductivity to $10–10^2$ S m^{-1}, and then active interconnected MnO_2 nanosheets were electrodeposited on the modified textiles. The textile electrodes with a 3D hierarchical branched structure enabled the Zn//MnO_2 battery to deliver a desirable energy density of 12 mWh cm^{-3} at 13 mW cm^{-3}, and capacity retention of over 80% after soaking in water for 200 min[57].

More interestingly, interconnected CNT bundles can assemble into 3D porous CNT foams as conductive frameworks to provide sufficient surface for the uniform growth of MnO_2 nanoparticles by $KMnO_4$ etching (Fig. 5a). Notably, as-fabricated MnO_2/CNT composite foam not only exhibited a high porosity of 98.4% to effectively buffer the volume variations and offer ion transfer pathways during MnO_2/Mn^{2+} redox deposition/dissolution processes (Fig. 5b), but also withstood 70% strain compression for repeated 200 times, indicative of extraordinary robustness and flexibility. Based on both MnO_2/Mn^{2+} and MnO_2/Mn^{3+} redox reactions due to the presence of 0.005 mol L^{-1} Mn^{2+} additive in the mild aqueous

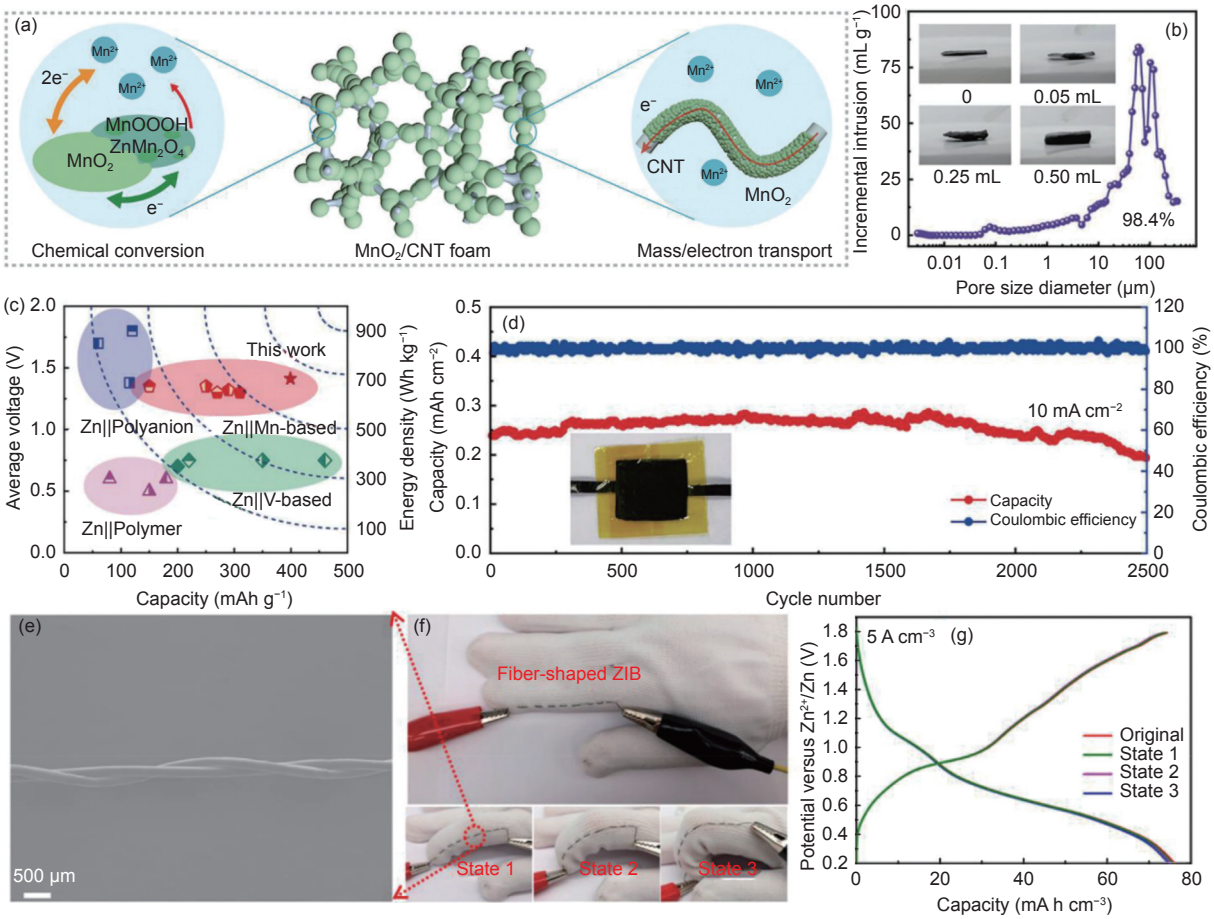

Fig. 5 (a) Schematic illustrating the MnO_2/CNT foam with reversible chemical conversion and hierarchical structure favoring mass/electron transport. (b) Pore size distribution of the MnO_2/CNT foam. (c) The capacity and average voltage of a ZIB assembled with MnO_2/CNT foam cathode in comparison with previously reported works on ZIBs. (d) Cycling stability of the constructed 3D sandwiched FZIB[58]. Reprinted with permission by copyright 2021, Wiley. (e) SEM image of a 1D fiber-shaped FZIB. (f) Digital photographs of a fiber-shaped FZIB woven into a glove at different bending states, and (g) corresponding GCD curves of the FZIB at 5.0 A cm^{-3}[53]. Reprinted with permission by copyright 2020, ACS.

$ZnSO_4$ electrolytes, the Zn//MnO_2 battery with a high discharge plateau displayed an energy density ($E_{material}$) of 602 Wh kg^{-1} (Fig. 5c), and ultralong lifespan of 16 000 cycles. Moreover, the assembled 3D sandwiched FZIB could maintain 83.5% of initial capacity after 2 500 cycles (Fig. 5d), and 2 connected batteries in series with an open-circuit of 3.8 V could power a rotor, indicative of the great potential for practical applications[58].

Besides, CNT based fibers possess superior mechanical strength, high conductivity, and light weight, which hold great promise in the construction of 1D FZIBs. Specially, CNT bundles were firstly prepared on Si wafers with the help of a Fe film catalyst through a typical floating catalytic chemical vapor deposition (CVD) method, which were further wound into CNT fibers with a diameter of 80-100 μm by dry-spinning. Subsequently, the as-fabricated CNT fibers were employed as current collectors for the electrochemical deposition of intertwined ε-MnO_2 nanosheets, and the diameter of MnO_2@CNT fibers increased by 20 μm after deposition. A 1D cable-type FZIB was constructed using a MnO_2@CNT fiber cathode, Zn wire anode, and $ZnCl_2$ based gel polymer electrolyte, which delivered a capacity of 290 mAh g^{-1} at 0.1 A g^{-1} and an energy density ($E_{material}$) of 360 Wh kg^{-1} at 100 W Kg^{-1}. More importantly, the 1D FZIB could realize stable charge/discharge process during 100 bending cycles[52]. Moreover, Wang and co-workers[53] twisted CNT belts to develop oxidized CNT fibers with hydrophilic surface for the uniform growth of 1D CNTs stitched 2D $Zn_3(OH)_2V_2O_7{\cdot}2H_2O$ (ZVO) nanosheets (Fig. 5e), which exhibited exceptional structural stability with a tensile strength of 280 MPa and enhanced conductivity of 98 S cm^{-1}. Specially, the interconnected CNT network and the open frameworks of layered ZVO jointly endowed the 1D fiber-shaped FZIB with a desirable volumetric density (E_{device}) of 71.6 mWh cm^{-3} and a desirable capacity retention of >96% after repeated 1 000 bending times. Moreover, the presence of flexible CNT fibers enabled the 1D fiber-shaped FZIB to be woven into various flexible fabrics and bent at different states without obvious capacity decay (Fig. 5f, g), showing their great promise in wearable electronics. In addition, ultrathin Co_3O_4 nanosheets (Co_3O_4 NSs) were proposed to be aligned on robust CNT fibers (CNTF) through in situ oxidation and etching of 3D Co-based metal organic framework arrays, and the resulting Co_3O_4 NSs@CNTF showed exceptional conductivity, which endowed the 1D fiber-shaped FZIB with a desirable reversible capacity of 158.70 mAh g^{-1} at 1 A g^{-1} and excellent capacity retention of 97.27% after 10 000 cycles. More interestingly, the as-constructed flexible batteries could be knitted into a sweater and be connected in series to power a watch[54]. Besides, spherical zinc hexacyanoferrate (ZnHCF) with particle sizes of less than 300 nm were arranged on compact CNT fibers, and the as-fabricated ZnHCF@CNT composite was served as outer cathodes to couple with Zn nanosheet arrays on a CNT fiber core, giving birth to a high-voltage coaxial 1D FZIB, which achieved a reversible capacity of 100.2 mAh cm^{-3} at 0.1 A cm^{-3}, an energy density of 195.4 mWh cm^{-3} at 0.2 W cm^{-3}, and a high capacity retention of 93.2% after 3 000 bending times[55].

CNTs with large aspect ratios are easily assembled into 1D CNT fibers, and thus are widely applied in 1D FZIBs[80]. CNT fibers as current collectors possess high conductivity to ensure rapid electron transfer, and meanwhile the functional groups on the surface of CNTs can enhance hydrophilic nature and interface stability between CNT based current collectors and active materials but would slightly sacrifice conductivity. Taking conductivity and stable structures into consideration, CNT fibers with both conductive core and functional groups may be a rational choice for the construction of robust electrodes and flexible FZIBs in the near future.

Despite the great progress of CNTs for FZIBs, the precise synthesis, assembly, and functionalization of CNTs are still challenging. Moreover, some important properties (e.g., high conductivity) should be ensured during their applications, meanwhile, CNTs may possess sufficient wettability with aqueous electrolytes for easy infiltration.

3.2.2 Carbon fibers

Generally, carbon fibers can be interwoven into carbon fiber cloth (CC) or be assembled into carbon nanofiber membrane by electrospinning. Carbon fiber cloth or membrane could be employed as light-weight and high-surface-area current collectors to load active material [81, 82].

Typically, high-capacity layered VSe_2 nanosheets on 1D N doped carbon nanofibers (N-CNFs) were synthesized by electrospinning, carbonization/oxidation, and selenization. The resulting core/shell nanostructures with strong interfacial interaction displayed high mechanical flexibility and excellent electrochemical properties. Moreover, to further stabilize the composite structure and alleviate dissolution issues of active materials during charge/discharge processes, atomic layer deposited Al_2O_3 layers with a thickness of ~5 nm uniformly covered VSe_2 nanosheets (Fig. 6a), forming Al_2O_3@VSe_2 NSs@N-CNFs films with an excellent tensile strength of 230 MPa. Accordingly, the 3D sandwiched FZIB showed a stack energy density of ~125 Wh kg^{-1} and high capacity retention of 86.2% after 2 500 cycles (Fig. 6b). Interestingly, the FZIBs could power an integrated soft robot to walk on land and even in water (Fig. 6c), which exploit multifunction ZIBs and broaden the applied fields of FZIBs[59].

In addition, directly growing active materials on

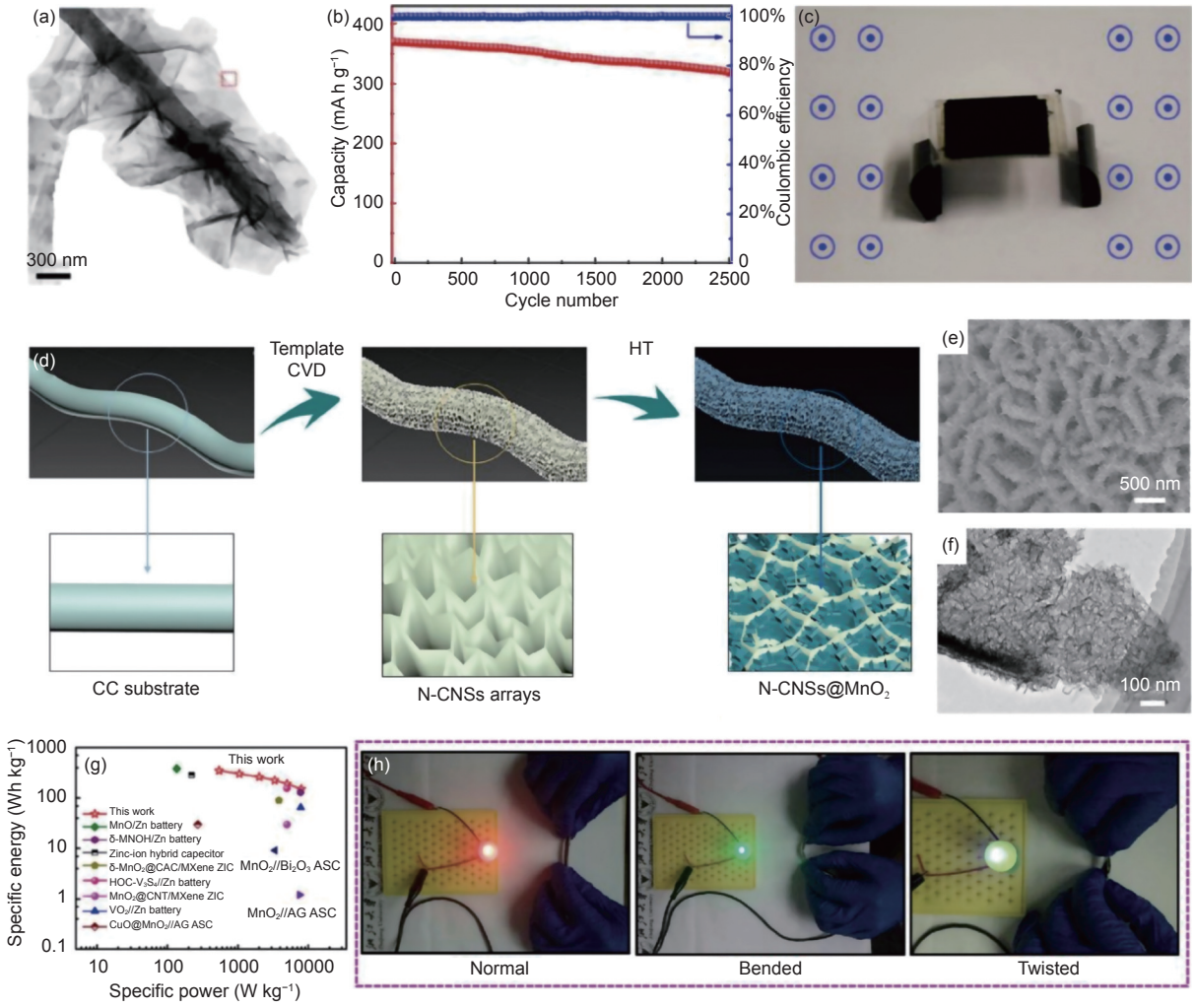

Fig. 6 (a) Transmission electron microscopy (TEM) image of Al_2O_3@VSe_2 NSs@N-CNF. (b) Cycling stability of a FZIB at 5.0 A g^{-1}. (c) The FZIBs could power an integrated soft robot[59]. Reprinted with permission by copyright 2022, Elsevier. (d) Schematic showing the fabrication of a flexible N-CNS@MnO_2 cathode. (e) SEM and (f) TEM images of N-CNSs@MnO_2. (g) Ragone plot of a N-CNS@MnO_2 based FZIB in comparison with previously reported flexible energy storage devices. (h) Digital images showing that N-CNSs@MnO_2 based ZIBs could power a table lamp and a light signboard[64]. Reprinted with permission by copyright 2020, Elsevier.

CC substrates could achieve a stable structure and avoid the use of polymer binders (e.g., polyvinylidene difluoride (PVDF)) in traditional cathodes. For example, metastable layered VO_2 (B) can store Zn^{2+} based on Zn^{2+} insertion/de-insertion. Carbon fiber sheets (CFSs) were reported as current collectors for the uniform and dense dispersion of VO_2 (B) arrays with a mass loading of 4.5 mg cm^{-2}, achieving a flexible VO_2 (B)@CFS composite. The stable adhesion between VO_2 and CFSs enabled two FZIBs connected in series to light up a small LED lamp for 150 h under different bending degrees ranging from 0° to 180°[60]. Moreover, VS_2 nanosheets with a thickness of 180 nm were densely grown on conductive CC current collectors with a high mass loading of 15.1 mg cm^{-2} for robust and flexible VS_2/CC cathodes by a facile hydrothermal strategy. With the use of self-healing poly(vinyl alcohol) (PVA)/$Zn(CH_3COO)_2$/$Mn(CH_3COO)_2$ hydrogel electrolytes, the 3D sandwiched FZIB showed stable capacities of 124, 125 and 114 mAh g^{-1} at 50 mA g^{-1} after 30 cycles at bending angles of 60°, 90° and 180°, respectively[61]. Besides, a hydrated zinc vanadium oxide/carbon cloth (ZnVOH/CC) composite was developed, in which ZnVOH nanosheets were uniformly and tightly anchored on the surface of CC by hydrothermal treatment and subsequent in situ electrochemical transformation. The strong connection between CC and ZnVOH ensured high structural stability and effectively suppressed the aggregation and dissolution issues of active materials. Meanwhile, the presence of structural water and lattice defects in 2D ZnVOH nanosheets provided abundant active sites and favored rapid reaction kinetics. Consequently, the FZIB delivered a reversible capacity of 184 mAh g^{-1} at 10 A g^{-1} after 170 cycles, and could work at rolled, folded or punched states[62].

Besides vanadium-based composites, manganese oxides can also be loaded on CC current collectors. For example, Tan et al.[63] used an in situ carbonization strategy of Mn-metal organic framework to synthesize oxygen defective Mn_3O_4@C nanorod arrays on CC substrates (O_d-Mn_3O_4@C NA/CC), in which oxygen defects not only adjusted the Mn^{3+} charge density for improved conductivity but also changed the MnO_6 octahedral structure, and thus enhanced structural stability and suppression of Mn dissolution could be simultaneously achieved. Moreover, the resultant carbon skeleton offered a conductive network for rapid electron transfer. Consequently, the corresponding ZIB achieved a long-term lifespan of 12 000 cycles and a capacity retention of 95.7% at 5 A g^{-1}. Moreover, with acetonitrile as a carbon source and MgO as a template, cross-linked N-doped carbon nanosheets (N-CNSs) could be grown on CC current collectors, which functioned as conductive and porous skeleton for the intimate decoration of MnO_2 nanoflakes for integrated N-CNS@MnO_2 arrays with a unique core/shell structure and extraordinary flexibility (Fig. 6d-f). The cross-linked and robust N-CNS arrays could not only provide large surface area to accommodate sufficient MnO_2 and abundant ion tunnels to favor Zn^{2+} diffusion, but also enrich active sites and enhance electron transfer by introducing N dopant. As expected, the 3D sandwiched FZIB delivered a high energy density of 352.5 Wh kg^{-1} at 542.4 W kg^{-1} (Fig. 6g), and can power LED lamp at normal, bent, and twisted states (Fig. 6h)[64]. Besides, zeolitic imidazole framework-67 (ZIF-67) that hydrothermally grown on CC could be converted to ultrathin MnO_2 nanosheet based hollow polyhedrons. The resultant robust MnO_2/CC composite exposed more active sites and reduced ion diffusion pathways, and thus the corresponding FZIB showed a reversible capacity of 91.7 mAh g^{-1} at 0.1 A g^{-1} and powered LED bulbs under bent states[65]. More interestingly, through the self-polymerization of dopamine, PDA layers stably adhered to CC substrates due to the presence of abundant catechol groups. Further, ultrathin δ-MnO_2 nanosheets were in situ grown on CC with strong interaction through the reaction between polydopamine derived N doped carbon and $KMnO_4$ ($4KMnO_4 + 3C + H_2O \rightarrow 4MnO_2 + K_2CO_3 + 2KHCO_3$). It should be noted that the remaining unreacted carbon network could effectively improve structural stability and accelerate electron transfer. Therefore, the free-standing

C-MnO_2@CC cathode could enable the 3D sandwiched FZIB to be bent at different angles without obvious capacity decay and deliver a high energy density of 1.34 mWh cm^{-2} at a power density of 2.95 mW cm^{-2}[66]. Furthermore, Chen et al. reported the hydrothermal growth of MnO_2 on carbon fibers (CFs) and the resulting MnO_2/CF cathodes were further assembled with a Zn/CF anode and a PVA/$ZnCl_2$-$MnSO_4$ polymer electrolyte to construct a FZIB, which exhibited a high tensile strength of 293 MPa and an energy density ($E_{material}$) of 181.5 Wh kg^{-1} at 0.31 kW kg^{-1}[67]. Besides, Cu^{2+} pre-intercalated δ-MnO_2 (CuMO) nanowires were hydrothermally fabricated on CC, in which Cu^{2+} could not only regulate electronic bandgap and ion state for enhanced electron/ion transfer but also stabilize the MnO_2 framework through the ionic bonds with oxygen atoms, thus enabling reversible and fast H^+/Zn^{2+} insertion/extraction processes and favorable capacity retention of 90.1% after 700 cycles at 5 A g^{-1}[27].

3.2.3 Graphene

Graphene nanosheets could assemble into 2D flexible free-standing films or 3D porous aerogels[83], which could be further employed as light-weight current collectors to load active materials for high-energy-density FZIBs. As a typical example, with the assistance of PVDF, graphene was interconnected into a flexible graphene film, which was further treated in HCl solution to generate abundant oxygen-containing functional groups on the surface of graphene. More interestingly, the graphene film could not only act as a current collector for enhanced electron transfer, but also function as a reducer in the reaction of H_2O + 3C + $4MnO_4^-$ = $4MnO_2$ + $2HCO_3^-$ + CO_3^{2-}, resulting in free-standing MnO_2 needles independently grown on functionalized graphene films (FSM@FGF). The flexible cathode with enhanced charge diffusion endowed the FZIB with a capacity of 145.6 mAh g^{-1} at 0.3 A g^{-1} and stable cycling performance under flat and folded states in water, demonstrative of great flexibility and water-proof properties for further practical applications[68].

4 Carbons in anodes

In traditional ZIBs, commercial Zn foils are frequently employed as both current collectors and Zn anodes simultaneously. Because excessive Zn is usually used, the energy density of traditional ZIBs is not so high. Meanwhile, conventional Zn foils with unsmooth surface in aqueous ZIBs suffer from serious dendrite growth caused by nonuniform electric fields/Zn^{2+} fluxes and possible side reactions between electrolytes and Zn[84]. To address the above challenges, carbon materials with excellent physicochemical properties are introduced to remarkably improve Zn anodes, and several roles of carbon materials can be summarized as follows:

(1) Current collectors for electrochemically deposited Zn. Lightweight and robust carbon materials can greatly improve energy density and enable high mechanical flexibility for FZIBs in comparison with excessive and rigid Zn foils.

(2) Host materials. Carbon materials with high conductivity and large SSA could reduce nucleation barriers, homogenize electric fields, and provide abundant zincophilic sites to induce uniform Zn nucleation and growth for dendrite-free Zn anodes.

The key roles of carbon materials in improved FZIBs are shown in Table 2.

4.1 Current collectors for Zn

4.1.1 Carbon nanotubes

Hollow multiwalled CNT arrays could be interwoven into a 3D conductive and porous CNT network on CC skeleton by a CVD method, which further acted as a robust current collector for Zn plating. CNT skeleton with a high conductivity and high SSA enabled a low nucleation overpotential and more homogeneous electric fields for dendrite-free anodes (Fig. 7a), which endowed the Zn//Zn symmetrical batteries with a reduced voltage hysteresis of 27 mV and long lifespan of 200 h at 2 mA cm^{-2}, together with a high depth of discharge of 28% (Fig. 7b), and the Zn//MnO_2 battery with a capacity of 167 mAh g^{-1} after 1 000 cycles (Fig. 7c). Moreover, the 3D Zn//MnO_2 battery with a high mechanical flexibility recorded high capacity retention of >97% under flat,

Table 2　A summary of carbon based anodes for FZIBs.

Role of carbons	Device configurations	Anode	Cathode	Electrolyte	Voltage range	Capacity	Capacity retention	Energy/power density	Flexibility	Ref.
Current collectors for Zn	2D planar	Zn microparticles	γ-MnO_2	2 M $ZnSO_4$ + 0.5 M $MnSO_4$	0.9–1.8 V	19.3 mAh cm^{-3} at 7.5 mA cm^{-3}	83.9% (1300 cycles)	17.3 mWh cm^{-3} 150 mW cm^{-3} ($E_{electrode}$)	Bent	[85]
	3D sandwiched	Zn/CNT	CNT-MnO_x@ poly (3,4-ethylenedio-xythiophene) (PEDOT)	PVA/LiCl-$ZnCl_2$-$MnSO_4$ gel	1.0–1.8 V	289 mAh g^{-1} at 2 mA cm^{-2}	88.7% (1000 cycles)	126 Wh kg^{-1} ($E_{material}$)	Bent, twisted	[86]
	3D sandwiched	Zn@Cu@ACC	MnO_2@ACC	1 M $ZnSO_4$	0.5–1.9 V	291.79 mAh g^{-1} at 0.5 A g^{-1}	94.8% (1000 cycles)	–	Bent	[87]
	3D sandwiched	Zn/CC	PANI	3 M $ZnCl_2$	0.7–1.7 V	1.24 mAh cm^{-2} at 0.2 mA cm^{-2}	94.83% (1500 cycles)	1.31 mWh cm^{-2} 0.29 mW cm^{-2}	Bent	[88]
	3D sandwiched	Zn@N-VG@CC	MnO_2@N-VG@CC	PVA/$Zn(CF_3SO_3)_2$	0.8–1.8 V	283.3 mAh g^{-1} at 1.0 A g^{-1}	80% (300 cycles)	371.24 Wh kg^{-1} 0.474 kW kg^{-1} ($E_{material}$)	Bent, twisted	[89]
Host materials for Zn	3D sandwiched	ZCN	CNT/MnO_2	2 M $ZnSO_4$ + 0.2 M $MnSO_4$	1–1.85 V	198.8 mAh g^{-1} at 0.2 A g^{-1}	107.0% (1000 cycles)	–	Bent	[90]
	3D sandwiched	Zn particles/CNTs/PVDF-HFP	MnO_2	2 M $ZnSO_4$ + 0.1 M $MnSO_4$	1.0–1.9 V	318.5 mAh g^{-1} at 0.3 A g^{-1}	65% (1000 cycles)	430.1 Wh kg^{-1}/ 4.02 kW kg^{-1}	Bent	[91]

Note: M: mol L^{-1}

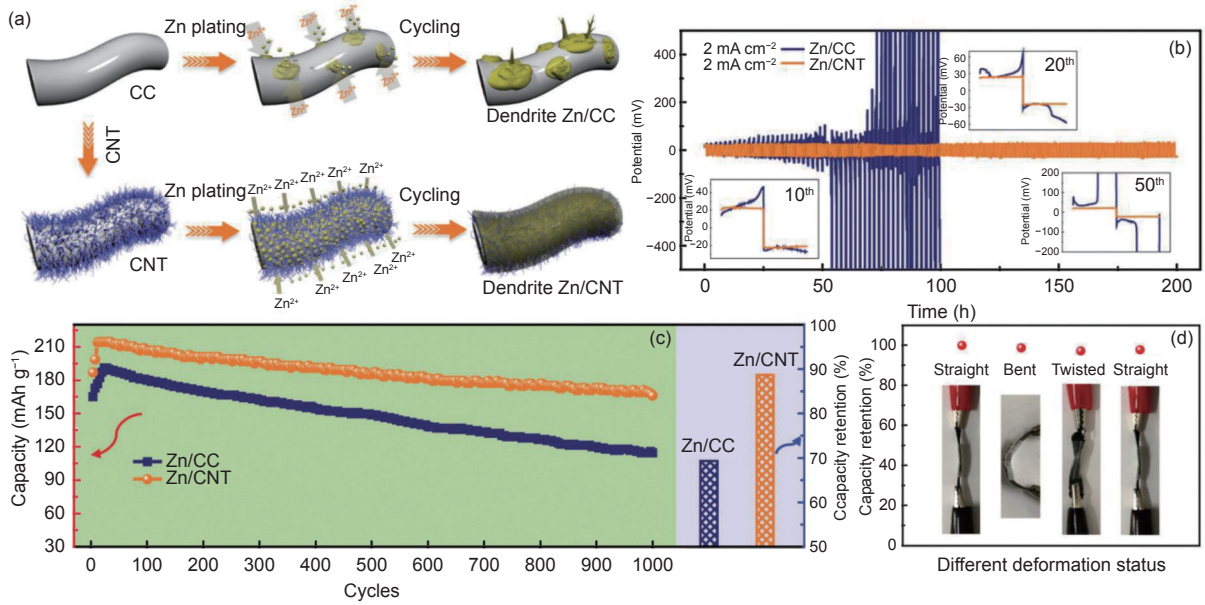

Fig. 7　(a) Schematic illustration of Zn deposition on CC and CNT substrates. (b) Cycling performance of Zn/CC and Zn/CNT anode based symmetrical batteries at 2 mA cm^{-2} and 2 mAh cm^{-2}. (c) Long-term cycling stability of a Zn/CNT//MnO_2 battery at 20 mA cm^{-2}. (d) Capacity retention of the flexible Zn/CNT//MnO_2 battery under different deformation states[86]. Reprinted with permission by copyright 2019, Wiley.

bent, or twisted states (Fig. 7d)[86]. In addition, Zn nanosheets (Zn NSs) could be electrodeposited on CNT fibers, and the Zn NSs@CNT fiber anode could offer abundant active sites, large surface area, and reduced ion diffusion path for reversible Zn/Zn^{2+} reaction kinetics and long cycling lifetime[53].

4.1.2　Carbon fibers

3D lightweight CC features high conductivity, desirable mechanical flexibility, and large SSA, and is considered as a promising current collector for electrodeposition of 1D Zn nanowires[61] and 2D Zn nanosheets. For example, Qian et al.[87] adopted activated carbon cloth (ACC) as a substrate for the vertical growth of zincophilic Cu nanosheets under a constant potential of −0.7 V for 600 s, which increased SSA from 36.85 m^2 g^{-1} of the bare ACC to 100.81 m^2 g^{-1} and favored the subsequent uniform Zn deposition for dendrite-free Zn@Cu@ACC anodes. The as-fabricated anodes could provide abundant active sites, accelerate charge transfer, and reduce the nucleation overpotential to 76 mV in comparison with ACC (214 mV), thus enabling the Zn//MnO_2 battery to

maintain a high capacity retention of 94.8% and Coulombic efficiency of 97.9% after 1 000 cycles at 1 A g^{-1}.

Moreover, Yuan and co-workers[88] selected commercial CC as a current collector for Zn nanoflake deposition, which further acted as a substrate for the encapsulation of polyacrylamide (PAm) hydrogel matrix through the cross-linking process of acrylamide monomer with N,N′-methylene-tcis-(acrylamide). Further, PANI with a high electronic conductivity of 1.4 S cm^{-1} was grown on the surface and embedded in the porous structure of a hydrogel host by in situ polymerization, and after it was soaked in $ZnCl_2$ electrolytes, the integrated and seamless configuration was obtained. This integrated architecture of designing batteries into an entity could not only avoid the use of excessive electrode additives and separator to enable a high energy density of 1.31 mWh cm^{-2} at 0.29 mW cm^{-2} but also ensure stable interface between electrode and electrolytes, endowing the integrated ZIB with a high flexibility to withstand frequent 3 000 bending cycles at an angle of 120°, accompanied with a high capacity retention of 97.75%. Notably, as-fabricated PAm hydrogel electrolyte with a porous and interconnected framework possessed a high ionic conductivity of 9.93 mS cm^{-1} at −20 °C, endowing the corresponding batteries with freeze-tolerance properties and operation at a wide temperature range from −20 to 20 °C, such as stable areal capacities of 1.148 mAh cm^{-2} at 20 °C, 0.964 mAh cm^{-2} at 0 °C, and 0.616 mAh cm^{-2} at −20 °C.

4.1.3 Graphene

Moreover, 2D graphene nanosheets could be easily assembled into 3D aerogel or foam, which are considered as an ideal current collector for Zn to enable enhanced electrolyte/electrode contact area, low local current density, and reduced side reactions at interface[89, 92]. Take a typical example, a flexible and ultralight $Ti_3C_2T_x$ MXene/graphene aerogel (MGA) was synthesized through hydrothermal assembly and freeze-drying (Fig. 8a, b), during which graphene nanosheets were interconnected into 3D frameworks and MXene nanosheets were uniformly decorated on the surface of graphene host. The MGA skeleton possessed a microporous structure and abundant zincophilic sites for dense electrodeposition of Zn (Fig. 8c, d). More importantly, the fluorine terminations of MXene could react with Zn to form zinc fluoride as solid electrolyte interface to induce uniform Zn nucleation for dendrite-free Zn anodes. As a result, the formation of by-products ($Zn(OH)_4^{2-}$) and hydrogen evolution reactions (3.8 mmol h^{-1} cm^{-2}) have been suppressed, and an ultralong life up to 1 000 h has been delivered at 10 mA cm^{-2} in a symmetrical battery. Furthermore, a 3D FZIB assembled with the $LiMn_2O_4$ cathode achieved an initial capacity of 110 mAh g^{-1} and maintained a capacity retention of 90.3% at 2 C at repeated folding times (Fig. 8e), together with intact structures without cracks at the folded position (Fig. 8f, g)[21]. Besides, 3D N-doped vertical graphene nanosheets (N-VG) with a size of ~400 nm were grown on CC through plasma-enhanced CVD and subsequent N doping, which acted as current collectors for Zn deposition to obtain robust and dendrite-free Zn@N-VG@CC anodes. Notably, the 3D graphene network could enable homogeneous electric fields and the introduction of zincophilic nitrogen-containing functional groups could strengthen the interfacial interaction between Zn^{2+} and CC, thus reducing Zn nucleation overpotential to 83 mV at 5 mA cm^{-2} and inducing uniform Zn nucleation. As a result, the flexible anodes endowed the FZIBs with a high capacity retention of more than 90% under bending and twisting states[89].

In addition, graphene featuring a high conductivity, stability, and desirable rheological properties could be screen-printed on flexible substrates for efficient electron transfer, which functioned as current collectors for the further screen-printing of highly conductive γ-MnO_2 ink (339 S m^{-1}) and Zn ink (463 S m^{-1}) as interdigital microelectrodes. As expected, the printed integrated 2D planar FZIB achieved a volumetric capacity ($E_{electrode}$) of 19.3 mAh cm^{-3} at 7.5 mA cm^{-3} and a volumetric energy density of 17.3 mWh cm^{-3} at 150 mW cm^{-3}, together with high mechanical flexibility to sustain various deformations, demonstrative of great promise in flexible microscale

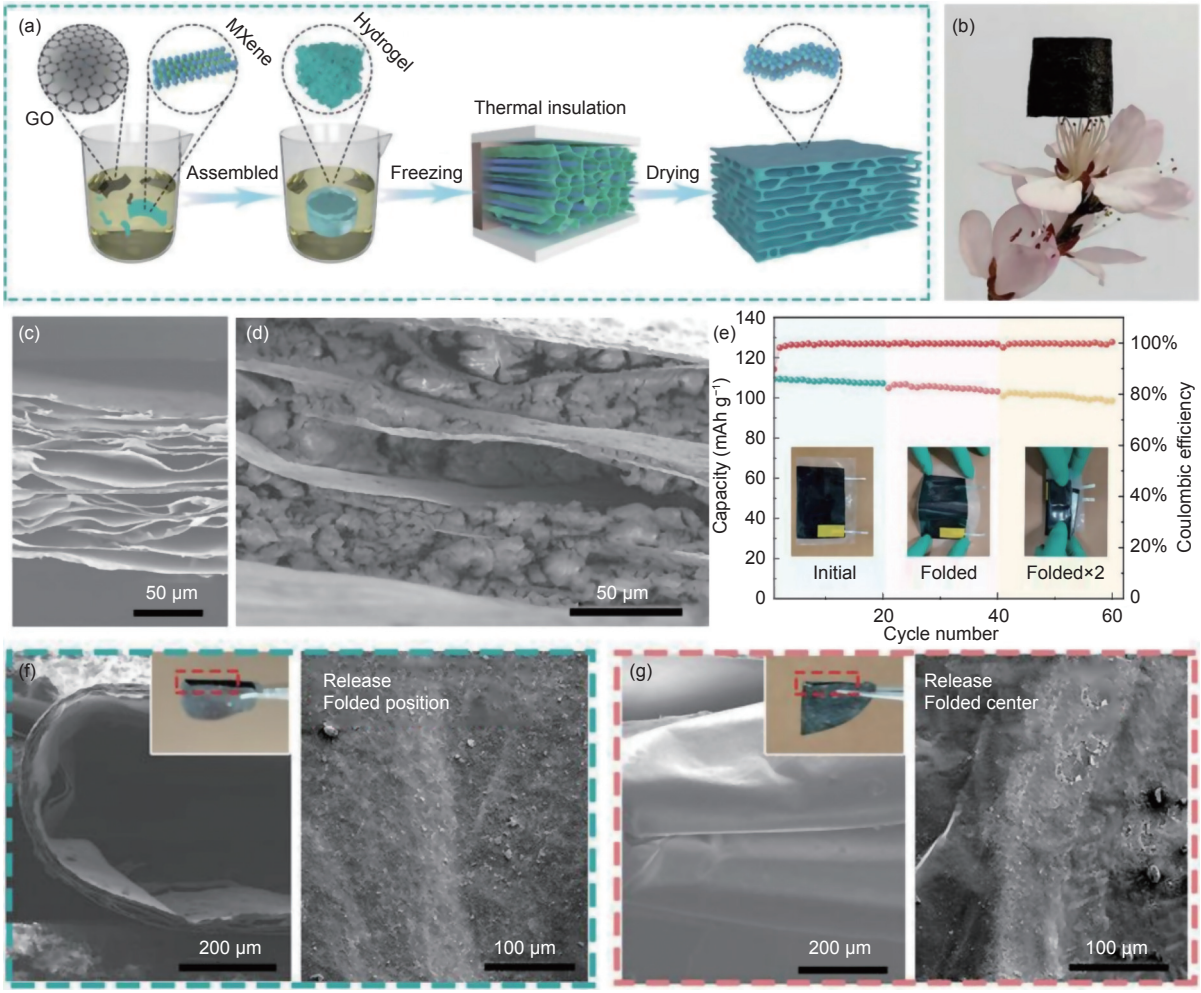

Fig. 8　(a) Schematic illustration showing the preparation of MGA. (b) Optical image of lightweight MGA. (c) SEM image of MGA. (d) SEM image of MGA after plating for 5 mAh cm^{-2}. (e) Cycling stability of a 3D $LiMn_2O_4$//MGA@Zn battery under different folded conditions. (f) SEM images of MGA after folding once and releasing. (g) SEM images of MGA after folding twice and releasing[21]. Reprinted with permission by copyright 2021, Wiley.

electronics[85].

4.2　Host materials for Zn

Lightweight and flexible carbon frameworks with large SSA could be used as hosts of nano/micro-structured Zn to homogenize electric fields and provide abundant zincophilic sites for Zn species without accumulation, thus enabling flexible and dendrite-free Zn anodes[8, 93]. Moreover, carbon materials (e.g., CNTs, graphene) could assemble with nano/micro-structured Zn particles and film-forming agent (e.g., nanocellulose) to construct flexible Zn films as an alternative to commercial Zn foils. As a typical example, uniformly dispersed zinc microspheres, CNTs, and nanocellulose were reported to be assembled into a free-standing ZCN film by a facile vacuum filtration method[90]. Notably, zinc powder with a microsphere structure could offer abundant electroactive sites and 3D diffusion pathways for reversible Zn plating/stripping, and conductive CNTs tightly connected with active materials could enlarge electroactive area and enable a low nucleation barrier of 52.6 mV at 1.0 mA cm^{-2}. Meanwhile, the introduction of nanocellulose enabled a flexible and bendable film with a strength of 3.61 MPa and a hydrophilic cathode favoring Zn^{2+} transfer. With a layer-by-layer vacuum filtration strategy, an integrated FZIB was constructed with the cellulose fiber film as a separator and the CNT/MnO_2 composite film as a cathode, which demonstrated stable operation for 1 000 cycles. Similarly, Wang et al.[91] prepared free-standing Zn anodes composed of active Zn particles, conductive CNTs, and mechanically flexible poly(vinylidene flu-

oride)-co-hexafluoropropylene (PVDF-HFP) by a spin-coating method. Zn particles with a diameter of ~13 μm can be embedded in 3D interconnected PVDF-HEP and CNT network for excellent flexibility and improved electrochemical performance, such as a high volumetric energy density (E_{device}) of 8.22 mWh cm^{-3} with a battery thickness of 0.4 mm. In addition, through a blade coating method, Zn microspheres with diameters of 3-5 μm were well dispersed on a 3D SWCNT and rGO network for a Zn/SWCNT-rGO film with a high conductivity of 597 S m^{-1}, in which rGO nanosheets had the ability to accommodate Zn species and meanwhile CNTs ensured high mechanical strength and rapid electron transfer[46]. Besides, with interfacial assembly of rGO on Zn foam and subsequent mechanical compression, graphene interpenetrated Zn (GiZn) hybrid foils were fabricated as dendrite-free anodes, in which conductive and hydrophilic rGO nanosheets provided abundant zincophilic sites to realize horizontal and uniform Zn deposition. Importantly, rGO nanosheets were well interpenetrated in Zn frameworks with strong interface, which enabled GiZn foils to be bent without breakages, showing great prospect in high-performance FZIBs[94].

5 Carbons in separators

As an essential component for a battery system, separators are used to prevent the direct contact between cathodes and anodes and thus avoid short-circuit issues. Moreover, separator engineering involving modification and functionalization is considered as a novel and efficient strategy for the construction of high-performance energy storage devices[95].

Generally, glass fiber (GF) separators are prevailing in aqueous ZIBs because of their hydrophilic nature, high ionic conductivity, and porous structure. In this respect, in situ modification of GF separators with conductive carbon materials, graphene in particular, offers an innovative avenue to improve the electrochemical performance of ZIBs. Typically, Li et al.,[96] used a plasma enhanced chemical vapor deposition (PECVD) strategy to grow 3D vertical graphene carpets on one side of GF separators to construct Janus separators with an ample porous structure and large SSA for uniform electric field and reduced local current density (Fig. 9a, b). Moreover, the introduction of oxygen and nitrogen functional groups could enhance zincophilicity to regulate homogeneous Zn^{2+} fluxes and stabilize Zn anodes. As a result, the robust Janus separators enabled the Zn//Zn symmetrical battery to stably cycle for 300 h at 0.5 mA cm^{-2} for 0.5 mAh cm^{-2} (Fig. 9c), and the Zn//V_2O_5 battery to deliver a high energy density of 182 Wh kg^{-1} and to withstand deformation without obvious electrochemical decay (Fig. 9d).

In addition, to further obtain low-cost separators, Wu and co-workers[97] proposed a functional cellulose nanofiber/graphene oxide (CG) separator, which possessed abundant pores within a range of 10-50 nm, smooth surface, and ample zincophilic oxygen containing functional groups to build strong interaction with Zn and enable uniform Zn^{2+} distribution for dendrite-free Zn anodes. More importantly, the CG separators could preferentially induce the hexagonal Zn growth along (002) plane owing to the low lattice mismatch of 7.4% between $Zn_{(002)}$ and $GO_{(002)}$ (Fig. 9e). As expected, the Zn//Zn symmetrical battery achieved an ultralong lifespan of 1 750 h with a low overpotential of 82 mV at 2 mA cm^{-2} and 1 mAh cm^{-2}, longer than counterpart with commercial glass fiber separators suffering from the limited cycling time of only 35 h (Fig. 9f). Moreover, the CG separators also enabled the 3D sandwiched flexible Zn//MnO_2/graphite full battery exhibiting a high energy density of 67 Wh L^{-1} and stable charge/discharge processes after bending for 500 times.

Despite the great progress so far, the research on carbons in separators is still in its infancy. Currently, the widely applied GF separators are fragile and possess large pores, which easily cause the occurrence of Zn dendrite growth and short circuits[98]. Moreover, little attention has been paid to the design of separator/electrolyte and separator/electrode interface, which defines the construction of FZIBs. In this respect, all-

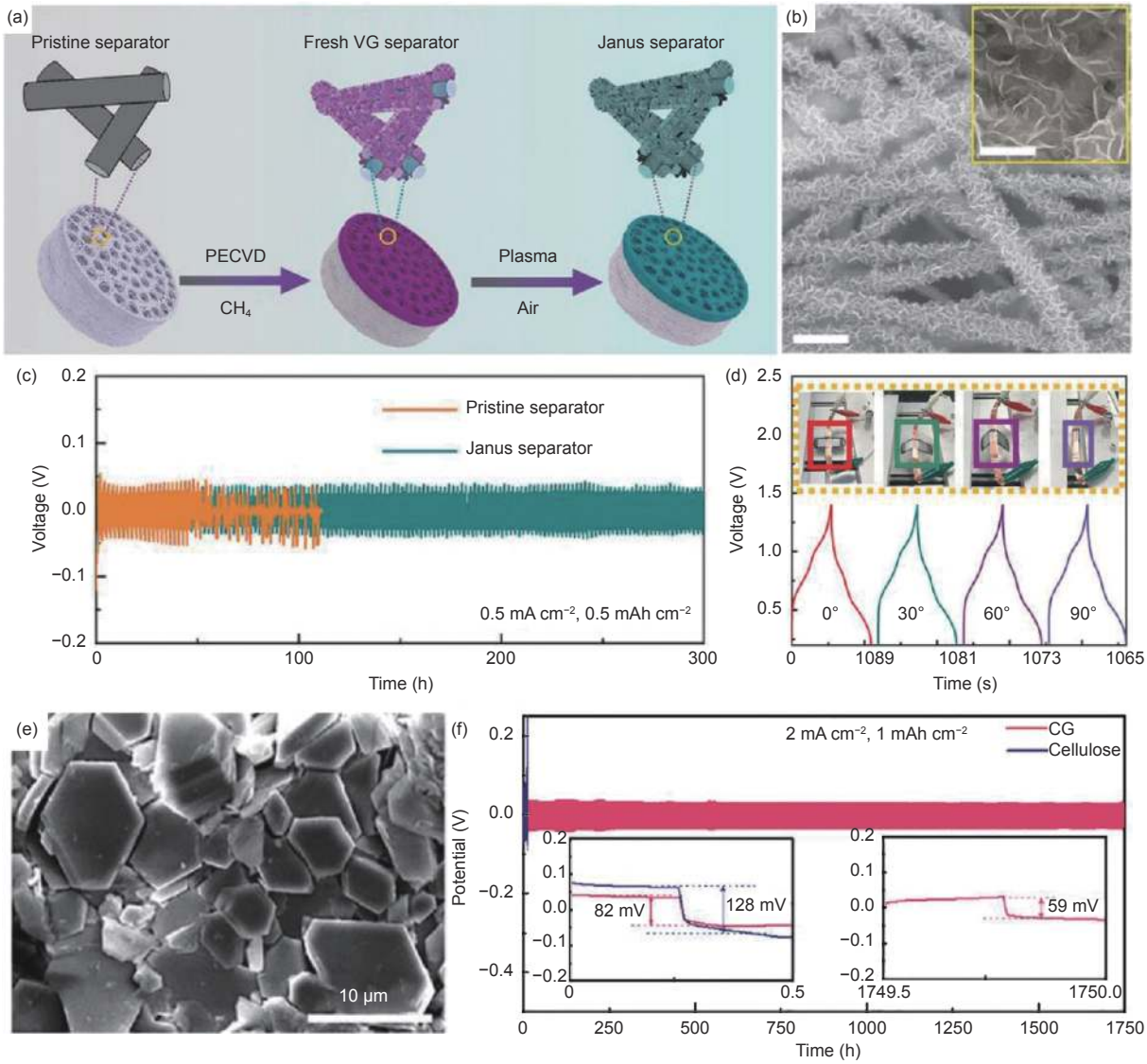

Fig. 9　(a) A Schematic showing the synthesis of a Janus separator. (b) SEM image of vertical graphene carpets on the Janus separator. (c) Cycling stability of Zn//Zn symmetrical batteries assembled with the Janus separator and pristine separator at 0.5 mA cm^{-2} for 0.5 mAh cm^{-2}. (d) Galvanostatic charge/discharge profiles of a Zn//V_2O_5 cell at 1 mA cm^{-2} at various bending angles[96]. Reprinted with permission by copyright 2020, Wiley. (e) SEM image of Zn anode in a CG separator based Zn//Zn battery after cycling at 2 mA cm^{-2}. (f) Cycling performance of Zn//Zn symmetrical batteries with CG and cellulose separators at 2 mA cm^{-2} and 1 mAh cm^{-2}[97]. Reprinted with permission by copyright 2021, Wiley.

in-one integrated system that combines all components into one monolith may be an effective strategy to stabilize interfaces and structures to have the ability to bear various deformations[99].

6　Conclusions and perspectives

This review summarizes the recent advancements of carbon materials (e.g., graphene, CNTs, carbon fibers) for FZIBs (e.g., 1D cable-shaped, 2D planar, and 3D sandwiched batteries), and the vital roles of carbon materials in constructing FZIBs are presented as conductive materials and current collectors for cathodes, current collectors and host materials for Zn, and functional separators. Notably, the fabrication strategy and the enhanced electrochemical performance and flexibility by carbon materials are specially emphasized. Despite great progress has been achieved, there are still much room for use of carbon materials in next-generation FZIBs.

(1) Rational selection and controllable synthesis of specific carbon materials for targeted configurations of FZIBs. Various carbon materials with unique physico-chemical properties could construct FZIBs

with different configurations. For example, CNTs with large aspect ratio are easily assembled into free-standing membrane or CNT fibers, which favors the design of 1D cable-shaped, 2D planar, 3D sandwiched FZIBs. Active materials could be directly grown on CC that constructed by carbon fibers, and thus CC are widely applied as current collectors for 3D sandwiched FZIBs. Highly stable and conductive graphene nanosheets could be interconnected into a porous network, which plays an important role in the achievement of 2D planar FZIBs. Furthermore, to construct stable interface between carbon materials and key battery materials, functionalization of carbon materials, generally introducing functional groups is usually employed for good adhesion and stable Zn^{2+} storage. Moreover, due to the use of aqueous electrolytes, carbon materials may possess appropriate hydrophilic properties in FZIBs for enhanced Zn^{2+} insertion/extraction while not ruining reaction kinetics[100]. Further, considering the construction of high-energy-density FZIBs, minimizing the mass ratio of carbon materials without sacrificing the sufficient roles of carbon materials for the flexibility and enhanced battery performance should be realized in FZIBs. In this regard, carbon material-based free-standing film electrodes may be a feasible way to effectively construct high-energy-density FZIBs. Besides, more carbon materials such as metal-organic frameworks derived carbon materials and graphdiyne also provide opportunities to construct advanced FZIBs[101–104], which have been rarely reported so far. Moreover, material genome engineering and simulation calculations may inject hopes into the development of new carbon materials and energy storage devices.

(2) Appropriate criteria to evaluate the flexibility of FZIBs should be established. Up to now, some standards such as the specific capacity, rate capability, cycling durability, energy density, and power density are widely used to evaluate the electrochemical performance of traditional ZIBs, in which the influence of both the depth of discharge and current density on the cycling life of FZIBs should not be ignored[105]. Besides, with regards to FZIBs, bending, twisting, and stretching tests are generally adopted to demonstrate excellent flexibility. However, the currently existing tests and geometry parameters are different and arbitrary, causing difficult comparison with different works and slow development of FZIBs. Therefore, it is essential to provide appropriate criteria to promote the smooth progress of FZIBs. For instance, Li et al.[11] proposed that the following three geometry parameters including the binding angle (θ), the bending radius of curvature (R), and the length of device (L) should be offered to precisely describe the bending states and characterize the FZIBs. Moreover, softness may be a standard to evaluate the wearability of FZIBs in order to fulfill the practical applications[11], such as wearable devices. Besides, precise mechanical computations may be introduced to analyze mechanical changes during various deformation conditions, which could be a base for the practical application of FZIBs.

(3) Rational construction of suitable battery configurations for targeted practical applications. Carbon materials with unique features are expected to construct FZIBs with diverse functionalities, such as electrochromic ZIBs[106] and photo rechargeable ZIBs[107]. To pursue the targets of FZIBs in diverse practical applications, the battery system should possess stable electrode/electrolyte interface, integrated battery structure, and superior device compatibility[108–111]. Significantly, the smart 1D cable-shaped FZIBs featuring superior wearability, can be directly employed as threads and woven into various flexible fabrics, or as textile electronics through the integration with display textiles for applications[29, 30]. More importantly, conventional fibers could be coated by GO layers, which may achieve reversible fusion and fission for wide-spread applications[112]. Moreover, 2D planar and 3D sandwiched FZIBs could be integrated with other electronics (e.g., solar cells, sensors, and nanogenerators) for the achievement of self-powered configuration, in which energy harvested could be directly consumed to drive the other flexible electronics. However, the exploration of FZIBs is still in the initial stage, and developing more configurations are

highly desired. In addition, some properties of FZIBs are desired for practical applications. For example, the shelf life, which indicates the storage time without use while not affecting the electrochemical performance of batteries, is usually neglected in the lab level[113], and this gap between lab and industrial level should be narrowed. Moreover, battery operation in extreme conditions (e.g., in a wide temperature range or in water) may be further explored in detail[3, 109, 114]. Besides, with the rapid evolution of 5G era, more techniques, such as machine learning may be introduced to the accurate design of intelligent FZIBs, which would bring hopes for the advancement of energy storage devices[24].

Overall, the introduction of carbon materials yields improved battery system with enhanced electrochemical performance and excellent mechanical flexibility. To keep pace with the ever-changing requirements, strenuous efforts should be further focused on the rational selection and controllable synthesis of specific carbon materials, appropriate criteria to evaluate the flexibility of FZIBs, and rational construction of suitable battery configurations for targeted practical applications.

Acknowledgements

This work was financially supported by LiaoNing Revitalization Talents Program (XLYC2007129), the Natural Science Foundation of Liaoning Province (2020-MS-095), the Fundamental Research Funds for the Central Universities of China (N2105008), and the fund of the State Key Laboratory of Catalysis in DICP (N-21-03).

References

[1] Dong H, Li J, Guo J, et al. Insights on flexible zinc-ion batteries from lab research to commercialization[J]. Advanced Materials, 2021, 33(20): 2007548.

[2] Li Y, Fu J, Zhong C, et al. Recent advances in flexible zinc-based rechargeable batteries[J]. Advanced Energy Materials, 2019, 9(1): 1802605.

[3] Zhang T, Tang Y, Guo S, et al. Fundamentals and perspectives in developing zinc-ion battery electrolytes: a comprehensive review[J]. Energy & Environmental Science, 2020, 13: 4625-4665.

[4] Olbasa B W, Fenta F W, Chiu S-F, et al. High-rate and long-cycle stability with a dendrite-free zinc anode in an aqueous Zn-ion battery using concentrated electrolytes[J]. ACS Applied Energy Materials, 2020, 3(5): 4499-4508.

[5] Li Y, Xie H, Wu G, et al. Study on performance of spinel $LiMn_2O_4$ derived from a high reactive Mn_2O_3 [J]. Chinese Journal of Rare Metals, 2020, 44(6): 616-621.

[6] Wu L, Dong Y. Recent progress of carbon nanomaterials for high-performance cathodes and anodes in aqueous zinc ion batteries[J]. Energy Storage Materials, 2021, 41: 715-737.

[7] Blanc L E, Kundu D, Nazar L F. Scientific challenges for the implementation of Zn-ion batteries[J]. Joule, 2020, 4(4): 771-799.

[8] Tang B, Shan L, Liang S, et al. Issues and opportunities facing aqueous zinc-ion batteries[J]. Energy & Environmental Science, 2019, 12(11): 3288-3304.

[9] Zhang N, Chen X, Yu M, et al. Materials chemistry for rechargeable zinc-ion batteries[J]. Chemical Society Reviews, 2020, 49(13): 4203-4219.

[10] Jia X, Liu C, Neale Z G, et al. Active materials for aqueous zinc ion batteries: synthesis, crystal structure, morphology, and electrochemistry[J]. Chemical Reviews, 2020, 120(15): 7795-7866.

[11] Li H, Tang Z, Liu Z, et al. Evaluating flexibility and wearability of flexible energy storage devices[J]. Joule, 2019, 3(3): 613-619.

[12] Kong L, Tang C, Peng H J, et al. Advanced energy materials for flexible batteries in energy storage: a review[J]. SmartMat, 2020, 1(1): 1-35.

[13] Zhang X, Jian W, Zhao L, et al. Direct carbonization of sodium lignosulfonate through self-template strategies for the synthesis of porous carbons toward supercapacitor applications[J]. Colloids and Surfaces A:Physicochemical and Engineering Aspects, 2022, 636: 128191.

[14] Zhang W, Jian W, Yin J, et al. A comprehensive green utilization strategy of lignocellulose from rice husk for the fabrication of high-rate electrochemical zinc ion capacitors[J]. Journal of Cleaner Production, 2021, 327: 129522.

[15] Yin J, Zhang W, Alhebshi N A, et al. Electrochemical zinc ion capacitors: fundamentals, materials, and systems[J]. Advanced Energy Materials, 2021, 11(21): 2100201.

[16] Wen F, Zhang W, Jian W, et al. Sustainable production of lignin-derived porous carbons for high-voltage electrochemical capacitors[J]. Chemical Engineering Science, 2022, 255: 117672.

[17] Chen Y, Xi B, Huang M, et al. Defect-selectivity and "order-in-disorder" engineering in carbon for durable and fast potassium storage[J]. Advanced Materials, 2022, 34(7): 2108621.

[18] Geng C, Chen Y, Shi L, et al. Design of active sites in carbon materials for electrochemical potassium storage[J]. New Carbon Materials, 2022, 37(3): 461-483.

[19] Chen Y, Shi L, Yuan Q, et al. Crystallization-induced morphological tuning toward denim-like graphene nanosheets in a KCl-copolymer solution[J]. ACS Nano, 2018, 12(4): 4019-4024.

[20] Xu G, Liu X, Huang S, et al. Freestanding, hierarchical, and

porous bilayered $Na_xV_2O_5·nH_2O$/rGO/CNT composites as high-performance cathode materials for nonaqueous K-ion batteries and aqueous zinc-ion batteries[J]. ACS Applied Materials & Interfaces, 2020, 12(1): 706-716.

[21] Zhou J, Xie M, Wu F, et al. Encapsulation of metallic Zn in a hybrid MXene/graphene aerogel as a stable Zn anode for foldable Zn-ion batteries[J]. Advanced Materials, 2022, 34: 2106897.

[22] Zhu Y, Yang X, Liu, et al. Flexible 1D batteries: recent progress and prospects[J]. Advanced Materials, 2020, 32(5): 1901961.

[23] Liu Y, Wang J, Zeng Y, et al. Interfacial engineering coupled valence tuning of MoO_3 cathode for high-capacity and high-rate fiber-shaped zinc-ion batteries[J]. Small, 2020, 16(11): 1907458.

[24] Shi X, Das P, Wu Z S. Digital microscale electrochemical energy storage devices for a fully connected and intelligent world[J]. ACS Energy Letters, 2021, 7(1): 267-281.

[25] Shi J, Wang S, Chen X, et al. An ultrahigh energy density quasi-solid-state zinc ion microbattery with excellent flexibility and thermostability[J]. Advanced Energy Materials, 2019, 9(37): 1901957.

[26] Yu P, Zeng Y, Zhang H, et al. Flexible Zn-ion batteries: recent progresses and challenges[J]. Small, 2019, 15(7): 1804760.

[27] Zhang R, Liang P, Yang H, et al. Manipulating intercalation-extraction mechanisms in structurally modulated δ-MnO_2 nanowires for high-performance aqueous zinc-ion batteries[J]. Chemical Engineering Journal, 2022, 433: 133687.

[28] Sun H, Zhang Y, Zhang J, et al. Energy harvesting and storage in 1D devices[J]. Nature Reviews Materials, 2017, 2(6): 1-12.

[29] He J, Lu C, Jiang H, et al. Scalable production of high-performing woven lithium-ion fibre batteries[J]. Nature, 2021, 597(7874): 57-63.

[30] Shi X, Zuo Y, Zhai P, et al. Large-area display textiles integrated with functional systems[J]. Nature, 2021, 591(7849): 240-245.

[31] Liao M, Wang C, Hong Y, et al. Industrial scale production of fibre batteries by a solution-extrusion method[J]. Nature Nanotechnology, 2022, 17(4): 372-377.

[32] Xiao X, Xiao X, Zhou Y, et al. An ultrathin rechargeable solid-state zinc ion fiber battery for electronic textiles[J]. Science Advances, 2021, 7(49): eabl3742.

[33] Sumboja A, Liu J, Zheng W G, et al. Electrochemical energy storage devices for wearable technology: a rationale for materials selection and cell design[J]. Chemical Society Reviews, 2018, 47(15): 5919-5945.

[34] Wang Z, Li Y, Wang J, et al. Recent progress of flexible aqueous multivalent ion batteries[J]. Carbon Energy, 2022, 4: 411-445.

[35] Bu F, Zhou W, Xu Y, et al. Recent developments of advanced micro-supercapacitors: design, fabrication and applications[J]. npj Flexible Electronics, 2020, 4(1): 1-16.

[36] Zheng S, Wang H, Das P, et al. Multitasking MXene inks enable high-performance printable microelectrochemical energy storage devices for all-flexible self-powered integrated systems[J]. Advanced Materials, 2021, 33(10): 2005449.

[37] Qu J, Zhang L, Song X, et al. Research progress of copper indium gallium selenide thin film solar cells. Chinese Journal of Rare Metals. 2020, 44(3): 313-327.

[38] Zhang Y, Zheng S, Zhou F, et al. Multi-layer printable lithium ion micro-batteries with remarkable areal energy density and flexibility for wearable smart electronics[J]. Small, 2021, 18: 2104506.

[39] Ma J, Zheng S, Cao Y, et al. Aqueous MXene/PH1000 hybrid inks for inkjet-printing micro-supercapacitors with unprecedented volumetric capacitance and modular self-powered microelectronics[J]. Advanced Energy Materials, 2021, 11(23): 2100746.

[40] Gao T, Yan G, Yang X, et al. Wet spinning of fiber-shaped flexible Zn-ion batteries toward wearable energy storage[J]. Journal of Energy Chemistry, 2022, 71: 192-200.

[41] Ren Y, Meng F, Zhang S, et al. CNT@MnO_2 composite ink toward a flexible 3D printed micro-zinc-ion battery[J]. Carbon Energy, 2022, 4: 446-457.

[42] Wang X, Li Y, Wang S, et al. 2D amorphous V_2O_5/graphene heterostructures for high-safety aqueous Zn-ion batteries with unprecedented capacity and ultrahigh rate capability[J]. Advanced Energy Materials, 2020, 10: 2000081.

[43] Song J, Wang W, Fang Y, et al. Freestanding CuV_2O_6/carbon nanotube composite films for flexible aqueous zinc-ion batteries[J]. Applied Surface Science, 2022, 578: 152053.

[44] Wang Y, Ye F, Wu Z, et al. Macroporous, freestanding birnessite $H_{0.08}MnO_2·0.7H_2O$ nanobelts/carbon nanotube membranes for wearable zinc-ion batteries with superior rate capability and cyclability[J]. ACS Applied Energy Materials, 2021, 4(4): 4138-4149.

[45] Wan F, Huang S, Cao H, et al. Freestanding potassium vanadate/carbon nanotube films for ultralong-life aqueous zinc-ion batteries[J]. ACS Nano, 2020, 14(6): 6752-6760.

[46] Yao M, Yuan Z, Li S, et al. Scalable assembly of flexible ultrathin all-in-one zinc-ion batteries with highly stretchable, editable, and customizable functions[J]. Advanced Materials, 2021, 33(10): 2008140.

[47] Bi S, Wu Y, Cao A, et al. Free-standing three-dimensional carbon nanotubes/amorphous MnO_2 cathodes for aqueous zinc-ion batteries with superior rate performance[J]. Materials Today Energy, 2020, 18: 100548.

[48] Li X, Li Y, Xie S, et al. Zinc-based energy storage with functionalized carbon nanotube/polyaniline nanocomposite cathodes[J]. Chemical Engineering Journal, 2022, 427: 131799.

[49] Wang J, Wang J G, Liu H, et al. A highly flexible and lightweight MnO_2/graphene membrane for superior zinc-ion batteries[J]. Advanced Functional Materials, 2021, 31: 2007397.

[50] Dai X, Wan F, Zhang L, et al. Freestanding graphene/VO_2 composite films for highly stable aqueous Zn-ion batteries with superior rate performance[J]. Energy Storage Materials, 2019, 17: 143-150.

[51] Guo Y, Zhao Z, Zhang J, et al. High-performance zinc-ion battery cathode enabled by deficient manganese monoxide/graphene

heterostructures[J]. Electrochimica Acta, 2022, 411: 140045.

[52] Wang K, Zhang X, Han J, et al. High-performance cable-type flexible rechargeable Zn battery based on MnO_2@CNT fiber microelectrode[J]. ACS Applied Materials & Interfaces, 2018, 10(29): 24573-24582.

[53] Pan Z, Yang J, Yang J, et al. Stitching of $Zn_3(OH)_2V_2O_7\cdot 2H_2O$ 2D nanosheets by 1D carbon nanotubes boosts ultrahigh rate for wearable quasi-solid-state zinc-ion batteries[J]. ACS Nano, 2020, 14(1): 842-853.

[54] Lu Y, Zhang H, Liu H, et al. Electrolyte dynamics engineering for flexible fiber-shaped aqueous zinc-ion battery with ultralong stability[J]. Nano Letters, 2021, 21(22): 9651-9660.

[55] Zhang Q, Li C, Li Q, et al. Flexible and high-voltage coaxial-fiber aqueous rechargeable zinc-ion battery[J]. Nano Letters, 2019, 19(6): 4035-4042.

[56] Huang A, Chen J, Zhou W, et al. Electrodeposition of MnO_2 nanoflakes onto carbon nanotube film towards high-performance flexible quasi-solid-state Zn-MnO_2 batteries[J]. Journal of Electroanalytical Chemistry, 2020, 873: 114392.

[57] Zhao T, Zhang G, Zhou F, et al. Toward tailorable Zn-ion textile batteries with high energy density and ultrafast capability: building high-performance textile electrode in 3D hierarchical branched design[J]. Small, 2018, 14(36): 1802320.

[58] Shen X, Wang X, Zhou Y, et al. Highly reversible aqueous Zn-MnO_2 battery by supplementing Mn^{2+}-mediated MnO_2 deposition and dissolution[J]. Advanced Functional Materials, 2021, 31(27): 2101579.

[59] Yang J, Yang H, Ye C, et al. Conformal surface-nanocoating strategy to boost high-performance film cathodes for flexible zinc-ion batteries as an amphibious soft robot[J]. Energy Storage Materials, 2022, 46: 472-481.

[60] Li X, Yang L, Mi H, et al. VO_2(B)@carbon fiber sheet as a binder-free flexible cathode for aqueous Zn-ion batteries[J]. CrystEngComm, 2021, 23(48): 8650-8659.

[61] Liu J, Long J, Shen Z, et al. A self-healing flexible quasi-solid zinc-ion battery using all-in-one electrodes[J]. Advanced Science, 2021, 8(8): 2004689.

[62] Tao Y, Huang D, Chen H, et al. Electrochemical generation of hydrated zinc vanadium oxide with boosted intercalation pseudocapacitive storage for a high-rate flexible zinc-ion battery[J]. ACS Applied Materials & Interfaces, 2021, 13(14): 16576-16584.

[63] Tan Q, Li X, Zhang B, et al. Valence engineering via in situ carbon reduction on octahedron sites Mn_3O_4 for ultra-long cycle life aqueous Zn-ion battery[J]. Advanced Energy Materials, 2020, 10(38): 2001050.

[64] Zhang Y, Deng S, Li Y, et al. Anchoring MnO_2 on nitrogen-doped porous carbon nanosheets as flexible arrays cathodes for advanced rechargeable Zn-MnO_2 batteries[J]. Energy Storage Materials, 2020, 29: 52-59.

[65] Wu F, Gao X, Xu X, et al. MnO_2 nanosheet-assembled hollow polyhedron grown on carbon cloth for flexible aqueous zinc-ion batteries[J]. ChemSusChem, 2020, 13(6): 1537-1545.

[66] Li F, Liu Y L, Wang G G, et al. The design of flower-like C-MnO_2 nanosheets on carbon cloth toward high-performance flexible zinc-ion batteries[J]. Journal of Materials Chemistry A, 2021, 9(15): 9675-9684.

[67] Chen J, Zhou Y, Islam M S, et al. Carbon fiber reinforced Zn-MnO_2 structural composite batteries[J]. Composites Science and Technology, 2021, 209: 108787.

[68] Lee Y G, Lee J, An G H. Free-standing manganese oxide on flexible graphene films as advanced electrodes for stable, high energy-density solid-state zinc-ion batteries[J]. Chemical Engineering Journal, 2021, 414: 128916.

[69] Li X, Wang X Y, Sun J. Recent progress in the carbon-based frameworks for high specific capacity anodes/cathode in lithium/sodium ion batteries[J]. New Carbon Materials, 2021, 36(1): 106-116.

[70] Bai Y, Yue H, Wang J, et al. Super-durable ultralong carbon nanotubes[J]. Science, 2020, 369(6507): 1104-1106.

[71] Liu X, Ma L, Du Y, et al. Vanadium pentoxide nanofibers/carbon nanotubes hybrid film for high-performance aqueous zinc-ion batteries[J]. Nanomaterials, 2021, 11(4): 1054.

[72] Tang F, Zhou W, Chen M, et al. Flexible free-standing paper electrodes based on reduced graphene oxide/δ-$Na_xV_2O_5\cdot nH_2O$ nanocomposite for high-performance aqueous zinc-ion batteries[J]. Electrochimica Acta, 2019, 328: 135137.

[73] Kim S H, Kim J M, Ahn D B, et al. Cellulose nanofiber/carbon nanotube-based bicontinuous ion/electron conduction networks for high-performance aqueous Zn-ion batteries[J]. Small, 2020, 16(44): 2002837.

[74] Liu X, Xu G, Huang S, et al. Free-standing composite of $Na_xV_2O_5\cdot nH_2O$ nanobelts and carbon nanotubes with interwoven architecture for large areal capacity and high-rate capability aqueous zinc ion batteries[J]. Electrochimica Acta, 2021, 368: 137600.

[75] Yue X, Liu H, Liu P. Polymer grafted on carbon nanotubes as a flexible cathode for aqueous zinc ion batteries[J]. Chemical Communications, 2019, 55(11): 1647-1650.

[76] Dong Y, Wu Z S, Ren W, et al. Graphene: a promising 2D material for electrochemical energy storage[J]. Science Bulletin, 2017, 62(10): 724-740.

[77] Li S, Liu Y, Zhao X, et al. Sandwich-like heterostructures of MoS_2/graphene with enlarged interlayer spacing and enhanced hydrophilicity as high-performance cathodes for aqueous zinc-ion batteries[J]. Advanced Materials, 2021, 33(12): 2007480.

[78] Shi F, Mang C, Liu H, et al. Flexible and high-energy-density Zn/MnO_2 batteries enabled by electrochemically exfoliated graphene nanosheets[J]. New Journal of Chemistry, 2020, 44(3): 653-657.

[79] Wang X, Wang L, Zhang B, et al. A flexible carbon nanotube@V_2O_5 film as a high-capacity and durable cathode for zinc ion batteries[J]. Journal of Energy Chemistry, 2021, 59: 126-133.

[80] Li H, Liu Z, Liang G, et al. Waterproof and tailorable elastic rechargeable yarn zinc ion batteries by a cross-linked polyacrylamide electrolyte[J]. ACS Nano, 2018, 12(4): 3140-3148.

[81] Shi H, Wen G, Nie Y, et al. Flexible 3D carbon cloth as a high-performing electrode for energy storage and conversion[J]. Nanoscale, 2020, 12(9): 5261-5285.

[82] Yang S, Cheng Y, Xiao X, et al. Development and application of carbon fiber in batteries[J]. Chemical Engineering Journal, 2020, 384: 123294.

[83] Hu H, Zhao Z, Wan W, et al. Ultralight and highly compressible graphene aerogels[J]. Advanced Materials, 2013, 25(15): 2219-2223.

[84] Zhang M, Xu W, Wu L, et al. Recent progress in MXene-based nanomaterials for high-performance aqueous zinc-ion hybrid capacitors[J]. New Carbon Materials, 2022, 37(3): 1-19.

[85] Wu Z S, Bao X, Sun C, et al. Scalable fabrication of printed Zn//MnO_2 planar micro-batteries with high volumetric energy density and exceptional safety[J]. National Science Review, 2020, 7(1): 64-72.

[86] Zeng Y, Zhang X, Qin R, et al. Dendrite-free zinc deposition induced by multifunctional CNT frameworks for stable flexible Zn-ion batteries[J]. Advanced Materials, 2019, 31(36): 1903675.

[87] Qian Y, Meng C, He J, et al. A lightweight 3D Zn@Cu nanosheets@activated carbon cloth as long-life anode with large capacity for flexible zinc ion batteries[J]. Journal of Power Sources, 2020, 480: 228871.

[88] Liu Y, Zhou X, Bai Y, et al. Engineering integrated structure for high-performance flexible zinc-ion batteries[J]. Chemical Engineering Journal, 2021, 417: 127955.

[89] Cao Q, Gao H, Gao Y, et al. Regulating dendrite-free zinc deposition by 3D zincopilic nitrogen-doped vertical graphene for high-performance flexible Zn-ion batteries[J]. Advanced Functional Materials, 2021, 31(37): 2103922.

[90] Wang A, Zhou W, Chen M, et al. Integrated design of aqueous zinc-ion batteries based on dendrite-free zinc microspheres/carbon nanotubes/nanocellulose composite film anode[J]. Journal of Colloid and Interface Science, 2021, 594: 389-397.

[91] Gao C, Wang J, Huang Y, et al. A high-performance free-standing Zn anode for flexible zinc-ion batteries[J]. Nanoscale, 2021, 13(22): 10100-10107.

[92] Chao D, Zhu C R, Song M, et al. A high-rate and stable quasi-solid-state zinc-ion battery with novel 2D layered zinc orthovanadate array[J]. Advanced Materials, 2018, 30(32): 1803181.

[93] Zhang Q, Luan J, Tang Y, et al. Interfacial design of dendrite-free zinc anodes for aqueous zinc-ion batteries[J]. Angewandte Chemie International Edition, 2020, 59(32): 13180-13191.

[94] Li Y, Wu L, Dong C, et al. Manipulating horizontal Zn deposition with graphene interpenetrated Zn hybrid foils for dendrite-free aqueous zinc ion batteries [J]. Energy & Environmental Materials, 2022.https://doi.org/10.1002/eem2.12423.

[95] Mo Y, Xiao K, Wu J, et al. Lithium-ion battery separator: functional modification and characterization[J]. Acta Physico-Chimica Sinica, 2022, 38(6): 2107030.

[96] Li C, Sun Z, Yang T, et al. Directly grown vertical graphene carpets as janus separators toward stabilized Zn metal anodes[J]. Advanced Materials, 2020, 32(33): 2003425.

[97] Cao J, Zhang D, Gu C, et al. Manipulating crystallographic orientation of zinc deposition for dendrite-free zinc ion batteries[J]. Advanced Energy Materials, 2021, 11(29): 2101299.

[98] Wu L, Zhang Y, Shang P, et al. Redistributing Zn ion flux by bifunctional graphitic carbon nitride nanosheets for dendrite-free zinc metal anodes[J]. Journal of Materials Chemistry A, 2021, 9(48): 27408-27414.

[99] Huang S, Wan F, Bi S, et al. A self-healing integrated all-in-one zinc-ion battery[J]. Angewandte Chemie International Edition, 2019, 58(13): 4313-4317.

[100] Zhang X, Li J, Ao H, et al. Appropriately hydrophilic/hydrophobic cathode enables high-performance aqueous zinc-ion batteries[J]. Energy Storage Materials, 2020, 30: 337-345.

[101] Gao X, Liu H, Wang D, et al. Graphdiyne: synthesis, properties, and applications[J]. Chemical Society Reviews, 2019, 48(3): 908-936.

[102] Yang Q, Li L, Hussain T, et al. Stabilizing interface pH by N-modified graphdiyne for dendrite-free and high-rate aqueous Zn-ion batteries[J]. Angewandte Chemie International Edition, 2022, 61(6): e202112304.

[103] Shen X, He J, Wang N, et al. Graphdiyne for electrochemical energy storage devices[J]. Acta Physico-Chimica Sinica, 2018, 34(9): 1029-1047.

[104] Chaikittisilp W, Ariga K, Yamauchi Y J J o M C A. A new family of carbon materials: synthesis of MOF-derived nanoporous carbons and their promising applications[J]. Journal of Materials Chemistry A, 2013, 1(1): 14-19.

[105] Li J, Lin Q, Zheng Z, et al. How is cycle life of three-dimensional zinc metal anodes with carbon fiber backbones affected by depth of discharge and current density in zinc-ion batteries?[J]. ACS Applied Materials & Interfaces, 2022, 14(10): 12323-12330.

[106] Wang Y, Jiang H, Zheng R, et al. A flexible, electrochromic, rechargeable Zn-ion battery based on actiniae-like self-doped polyaniline cathode[J]. Journal of Materials Chemistry A, 2020, 8(25): 12799-12809.

[107] Deka Boruah B, Mathieson A, Park S K, et al. Vanadium dioxide cathodes for high-rate photo-rechargeable zinc-ion batteries[J]. Advanced Energy Materials, 2021, 11(13): 2100115.

[108] Li H, Han C, Huang Y, et al. An extremely safe and wearable solid-state zinc ion battery based on a hierarchical structured polymer electrolyte[J]. Energy & Environmental Science, 2018, 11(4): 941-951.

[109] Mo F, Liang G, Meng Q, et al. A flexible rechargeable aqueous zinc manganese-dioxide battery working at −20 °C[J]. Energy & Environmental Science, 2019, 12(2): 706-715.

[110] Shao Z, Cheng S, Zhang Y, et al. Wearable and fully

biocompatible all-in-one structured "paper-like" zinc ion battery[J]. ACS Applied Materials & Interfaces, 2021, 13(29): 34349-34356.

[111] Zhang Y, Wang Q, Bi S, et al. Flexible all-in-one zinc-ion batteries[J]. Nanoscale, 2019, 11(38): 17630-17636.

[112] Chang D, Liu J, Fang B, et al. Reversible fusion and fission of graphene oxide-based fibers[J]. Science, 2021, 372(6542): 614-617.

[113] Chen Z, Li X, Wang D, et al. Grafted MXene/polymer electrolyte for high performance solid zinc batteries with enhanced shelf life at low/high temperatures[J]. Energy & Environmental Science, 2021, 14(6): 3492-3501.

[114] Jin X, Song L, Dai C, et al. A self-healing zinc ion battery under −20 °C[J]. Energy Storage Materials, 2022, 44: 517-526.

炭材料在柔性锌离子电池中的研究进展

武丽莎，　张明慧，　徐　文，　董琰峰*

（东北大学，理学院化学系，辽宁 沈阳 110819）

摘　要： 近年来，随着智能可穿戴设备市场的不断增长，柔性储能器件的设计和开发得到了快速发展。水系锌离子电池（ZIBs）具有成本低、高安全等优势，得到了广泛研究。炭材料具有质轻、高导电与柔性等特点，在构筑高性能柔性锌离子电池（FZIBs）方面具有诸多优势。本文详细总结了炭材料（碳纳米管、炭纤维、石墨烯）在一维线状、二维平面、三维三明治构型 FZIBs 中的研究进展，着重强调了炭材料构筑 FZIBs 的策略，系统归纳了炭材料在正极、负极和隔膜中的角色，重点强调了炭材料对 FZIBs 的性能增强作用。最后，简要讨论了先进炭材料在下一代柔性锌离子电池中的挑战和前景。

关键词： 炭材料；柔性锌离子电池；正极；负极；隔膜

文章编号： 1007-8827(2022)05-0827-25　　**中图分类号：** TQ127.1^{+}1　　**文献标识码：** A

基金项目： 辽宁省“兴辽英才计划”青年拔尖人才 (XLYC2007129); 辽宁省自然科学基金 (2020-MS-095); 中央高校基本科研业务费 (N2105008); 催化基础国家重点实验室基金 (N-21-03).

通讯作者： 董琰峰, 副教授. E-mail: dongyanfeng@mail.neu.edu.cn

作者简介： 武丽莎, 硕士研究生. E-mail: 1970065@stu.neu.edu.cn

本文的电子版全文由 Elsevier 出版社在 ScienceDirect 上出版（https://www.sciencedirect.com/journal/new-carbon-materials/）